Electrochimica Acta 113 (2013) 390–406

Contents lists available at ScienceDirect

Electrochimica Acta

journal homepage: www.elsevier.com/locate/electacta

Corrosion behavior of carbon steel in presence of sulfate-reducing bacteria in seawater environment

Marko Stipaničev[a,c,*], Florin Turcu[a], Loïc Esnault[a], Elmar Werner Schweitzer[b], Renate Kilian[b], Régine Basseguy[c]

[a] Det Norske Veritas, Johan Berentsens vei 109-111, Laksevåg, 5163 Bergen, Norway
[b] AREVA GmbH, PTCM-G, Paul-Gossen-Str. 100, 91052 Erlangen, Germany
[c] Laboratoire de Génie Chimique CNRS-INPT, 4 Allée Emile Monso, 31432 Toulouse, France

ARTICLE INFO

Article history:
Received 11 July 2013
Received in revised form 30 August 2013
Accepted 10 September 2013
Available online 6 October 2013

Keywords:
Seawater
Carbon steel
Corrosion
SRB

ABSTRACT

The influence of sulfate-reducing bacteria (SRB) on the corrosion behavior of carbon steel was studied in a laboratory test-loop, continuously fed with nutrient supplemented North Sea seawater. The main parts of the test-loop, represented by two separated flow cells, were fitted with steel specimens. The test-loop was operating anoxically for 2200 h and each flow cell was three times inoculated with *Desulfovibrio alaskensis* or *Desulfovibrio desulfuricans* species. Additionally, each flow cell was two times perturbed with antimicrobial treatments. Steel specimens exposed in flow cells exhibited comparable appearance and systems responding similarly to inoculations and antimicrobial treatments. The effect of the inoculations in both flow cells on the steel coupons electrochemical behavior was materialized as lower resistance to corrosion and higher surface activity or occurrence of localized pitting events. The localized surface attacks recognized in both flow cells after inoculations continued to progress with the time, although bacterial activity was temporarily suppressed by antimicrobial treatment. Post-exposure sample evaluations might suggest that, some particular steel surface areas have been subjected to a dramatic change in the corrosion mechanism from initial localized attack to general corrosion. The long-term exposure of the carbon steel specimens resulted in identifiable formation of biofilms and corrosion products. Corrosion deposits were characterized by a specific structure built of iron sulfides (FeS), sulfated green rust ($GR(SO_4^{2-})$), magnetite (Fe_3O_4), Fe(III) oxyhydroxides (FeOOH), chukanovite ($Fe_2(OH)_2CO_3$), carbonated green rust ($GR(CO_3^{2-})$) and some calcareous deposits. Presented factual evidence reinforced the idea that sulfidogenic species in natural seawater environment may cause localized damage with a specific surface pattern; however, this does not necessarily lead towards significantly elevated corrosion rates.

1. Introduction

Internal corrosion causes immense damages to the carbon steel offshore infrastructures such as pipelines and water injection systems. A significant part of the carbon steels degradation can be attributed to micro- and macro-environmental conditions alterations by sulfidogenic, e.g. hydrogen sulfide (H_2S) producing, microorganisms [1]. The most recognized group of sulfidogenic microorganisms are sulfate-reducing bacteria (SRB) and they are regarded as the main culprits of anaerobic corrosion in seawater system.

Within the marine biofilm matrix, SRBs thrive, finding favorable conditions inside pre-established anoxic niches. In general, SRB including *Desulfovibrio desulfuricans* ATCC 27774 and *Desulfovibrio alaskensis* AL1, are performing dissimilatory reduction of sulfur compounds such as sulfate (SO_4^{2-}), sulfite (SO_3^{2-}), thiosulfate ($S_2O_3^{2-}$), polythionate ($S_nO_6^{2}$) and sulfur (S) itself to sulfide (S^{2-}), that, combined with oxidized molecular hydrogen, forms volatile H_2S negatively impairing ferrous metals [2–4].

Anaerobic corrosion is a well-understood process, exclusively controlled by the oxidizing agent/proton transfer to metal surface. However, in biotic environments different explanations were suggested in order to explain anaerobic corrosion process that resulted in elevated corrosion rates. During past few decades multiple theories explaining corrosion mechanisms were suggested by taking into account SRBs metabolic activities and formation of different sulfide based compounds.

Earlier work evoked a cathodic depolarization model of ferrous metals based on the removal from the surface of atomic hydrogen by SRBs [5] and/or hydrogen consumption thanks to a hydrogenase enzyme [6–9]. This hypothesis was investigated and can be

* Corresponding author. Tel.: +47 95936347.
E-mail addresses: Marko.Stipanicev@dnv.com, marko.stipanicev@gmail.com (M. Stipaničev).

0013-4686/$ – see front matter © 2013 Elsevier Ltd. All rights reserved.
http://dx.doi.org/10.1016/j.electacta.2013.09.059

approved only if the reaction step for forming atomic (and then molecular) hydrogen is not rate-limiting as it is the case in presence of weak acid, especially when phosphate protonated species are involved [10,11]; it was then proved that bacterial hydrogen uptake merely stimulates corrosion in certain anaerobic environments [12]. Furthermore, by reducing sulfate in sulfide, SRB promotes the conditions for precipitation of iron sulfide (biomineralized Fe_xS_y, particularly FeS), which next catalyzes proton/water reduction into molecular hydrogen and acts as a cathode in a galvanic couple with metallic iron [13–15]. What's more, direct products of SRB metabolism, e.g. H_2S, can affect metal surface directly by decreasing pH locally and promoting differential cell resulting with localized events on metal surface [16]. Metal ion chelating by extracellular polymeric substances (EPS) is also sometimes dealt with [17] as well as galvanic coupling resulting EPS selective metal binding capacity [18]. To sum-up such a complex *marine biofilm/corrosion products/metal* interface, overlapping of proposed mechanisms should be considered rather than one specific mechanism [19]. It is often observed that the microenvironment generated within marine biofilms rich in SRB is favoring electrochemical reactions that may lead to localized destructive surface events [20]. Nevertheless, besides its detrimental impact on steel integrity, the biomineralization process occurring on steel surfaces can be under favorable circumstances beneficial thought the formation of protective corrosion products layers that can suppress the local corrosion processes [21].

Even though SRBs are recognized as the most imminent species taking part in microbiologically influenced corrosion (MIC), microbial consortiums in marine biofilms are usually heterogeneous and therefore deterioration of metal should be affected by interactions of the whole community [22]. Some of the microorganisms commonly found in marine environments, such as acid producing bacteria (APB) of the genera *Clostridia* [23,24] or *Anaerobaculum* [25], can be characterized by metabolic process capable of generating multiple, aggressive chemical species for ferrous metals, such as H_2S and CO_2. Furthermore, when dealing with MIC, it is required to take into consideration effect of other bacteria than SRB inside marine biofilms and possible quorum sensing effect, which according to authors knowledge, is still neither well investigated nor well defined.

Besides the evaluation of the bacterial load, the relevant characteristics of the metallic substrate, whose corrosion resistance in presence of microorganisms is investigated, must be known or taken into consideration. Carbon steels, often used in Oil and Gas (O&G) industry, are characterized by homogenous distribution of geometrically small grains that have short grain boundaries. This particular microstructure may result in surface susceptibility to equally allocated localized corrosion attack. For carbon steels, most common metallographic structures are ferrite (ferrous phase) and perlite (lamellar structure of ferrite and Fe_3C), with nonmetallic inclusions, e.g. manganese sulfide (MnS) inclusions randomly distributed over the steel surface. These MnS inclusions have been postulated to serve as seeds for pitting corrosion [26,27]. Recently, different studies showed a correlation between pit initiation and propagation associated with sulfide inclusions and their relation to MIC [28].

In order to get better insight in the complexity of systems such as biofilms, and their interactions with carbon steel surfaces, taking advantages of multiple analytic techniques may be useful. Currently, electrochemical techniques such as open circuit potential (OCP), linear polarization resistance (LPR) and electrochemical noise (EN) are widely employed for studying general and localized surface events in the presence of the bacteria and biofilms [29,30]. More precisely, LPR is often used to monitor corrosion by measuring "instantaneous" general corrosion rate [31], taking additional precaution due to the limitation of Stern–Geary theory, which is not valid for the diffusion-controlled systems that are often established in presence of biofilms. Localized events (pitting, crevice, stress corrosion...) are studied by electrochemical noise (EN). Iverson originally applied electrochemical current noise (ECN) and electrochemical potential noise (EPN) fluctuations as a tool for MIC studying and monitoring [32,33]. Until now, observations of the modulated current and potential signals patterns as well as the characteristic transients in the time records were successfully used for detection of stable and metastable localized surface events in the presence of bacteria and/or biomineralization products [31,34,35].

In the investigation reported herein, corrosion behavior of S235JR carbon steel was studied in the modified North Sea seawater that was multiple times inoculated with one of two different SRB pure cultures, *D. alaskensis* AL1 or *D. desulfuricans* ATCC 27774, and subjected to antimicrobial treatment. LPR and EN techniques were used in order to study general corrosion, and for identification of localized events on steel surfaces. Scanning Electron Microcopy (SEM) and Energy-Dispersive X-Ray (EDX) spectroscopy were used to investigate biomineralization products and processes governed by presence of bacteria. Surface deterioration and influence of microstructure on degree and location of corrosion attack were investigated by means of optical microscopy.

2. Methodology, materials and methods

2.1. Continuously fed with fresh media test loop

The main components of the continuously fed with fresh media test loop (also called "once-through" flow loop) were manufactured in-house and consist of two bioreactor vessels placed one behind the other and two in parallel cylindrical flow-through cells. The "once-through" flow loop set-up is depicted in Fig. 1.

The bioreactor vessels are made of polypropylene. The acryl lid, used for closing bioreactor vessels, is fitted with an optical oxygen-dipping probe, a temperature sensor interfaced with Fibox 3 fiber optic oxygen transmitter (Presens, Germany), one gas inlet, one gas outlet and a pH electrode (pH-meter HI-9125N, Hanna Norden AB, Sweden). The lid also incorporates an in-house fitted sampling/fluid injection point. The first bioreactor vessel body was fitted with one fluid injection inlet. Each bioreactor vessel was equipped with one fitting accommodating Teflon tube (Swagelok, UK) via which the two bioreactor vessels were connected. The second bioreactor vessel was also equipped with a heating unit (ISOPAD IP-DASI®, Tyco, USA) and a thermostat (Raychem® AT-TS-14, Tyco Thermal Controls, USA).

A peristaltic pump (W–M 520SN/REL, Watson–Marlow, UK) drew media from the second bioreactor vessel, and the output flow was split between the two flow cells. Perfluoroalkoxy tubing (PFA-T8-062-50, Swagelok, UK) was used. Two regulation needle valves (PFA-4RPS8, Swagelok, UK) were installed before and after each flow cell. Flow cells were made from acrylic tubes (6 cm inner diameter, 1 cm wall thickness and 34 cm length) and acrylic plates (5 cm × 34 cm × 0.5 cm). Twelve pairs of feedthroughs (M20 size fittings, produced by OBO Bettermann, Germany) were installed on the top of each flow cell. A schematic drawing of a flow cell showing its cross section and distribution of feedthroughs is presented in Fig. 2. Electrodes (working—WE, counter—CE and reference—Ref) for electrochemical measurements were installed in the two flow cells, in identical arrangements at 12 o'clock positions. An in-house manufactured liquid sampling port (SP) that accommodated dipping oxygen probe was installed at F10 position in each flow cell. To monitor biofilm formation, ten carbon steel specimens (rectangular plates with dimensions of a 1 cm × 1 cm × 0.2 cm) were installed at 6 o'clock position in each flow cell.

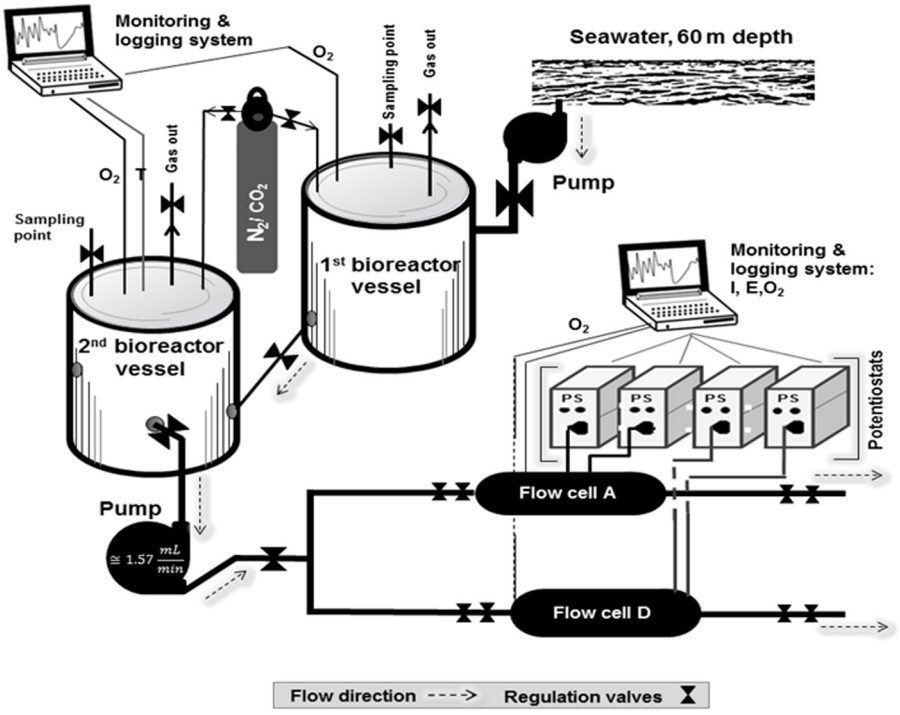

Fig. 1. The continuously fed with fresh media test loop.

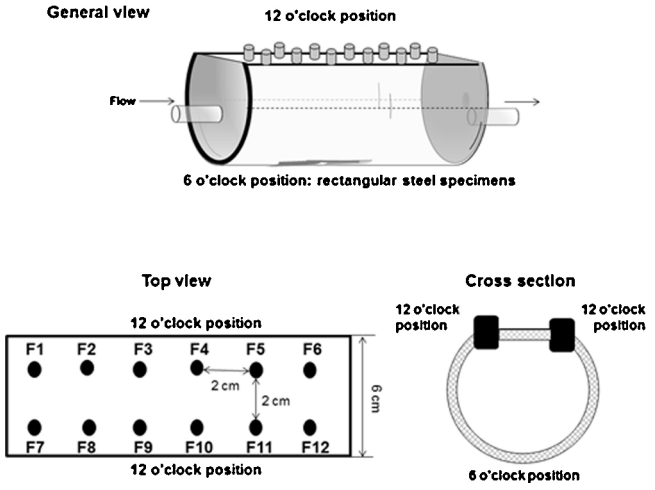

Fig. 2. Scheme, cross-section and fitting distribution of cylindrical flow-through cells, e.g. flow cells.

The entire "once-through" flow loop was constructed from polymers to minimize contamination with exogenous metal ions. Furthermore, materials, including perfluoroalkoxy (2 mm thickness), polyolefin (1 mm thickness), polypropylene (2 cm thickness) and acrylic (0.5 cm and 2 cm thickness) polymers with minimal oxygen permeability and minimal deterioration under test conditions were chosen.

Prior to operation the bioreactor loop was flushed with technical grade alcohol (Kemetyl Norge AS, Norway) and flow cells were exposed for 24 h under UV light (wave length 256 nm: XX-15, sterilization UV lamp, UVP, USA). Then, the first bioreactor vessel was filled up with 40 L of seawater, and oxygen was decreased to a level of 30–40 ppb by purging with 90/10 (v/v)% N_2/°O_2 gas mixture (Yarapraxiar, Norway) for 24 h. Deareated seawater was then transferred into the degassed second bioreactor vessel where the medium was supplemented with acetate (Merck, Germany) and lactate (Sigma-Aldrich, Germany) up to final concentrations of 10 μmol L^{-1}. Anoxic conditions (10–20 ppb) were established by purging the medium with 90/10 (v/v) % N_2/CO_2 gas mixture for 72 h. Moreover, the temperature was controlled automatically at 28 °C ± 2 °C during whole duration of test. The medium pH inside the second bioreactor vessel was adjusted with phosphate buffer (Sigma-Aldrich, Germany) to values in range of 7.9 to 8.1 before being distributed into the two separated flow cells. The flow system was then activated with a flow rate maintained at 1.57 mL min^{-1}, the lowest possible value for the pump. The continuously fed with fresh media test loop was operated continuously for the next 2200 h. Three time inoculations (with 100 mL at t_e = 792 h, t_e = 936 h and t_e = 1056 h) were performed using pure culture of *D. alaskensis* strain AL1 in flow cell A and *D. desulfuricans* strain ATCC 27774 in flow cell D. Prior to each inoculation, flow cells were isolated from the rest of the loop by closing regulation valves. Flow conditions were reestablished 24 h after each inoculation. Moreover, each flow cell was two times treated with 50 min batch antimicrobial treatment, first after the third inoculation, at t_e = 1075 h and second time at t_e = 2180 h. A 50% glutaraldehyde solution (MB-544 C from M-I SWACO a Schlumberger Company, USA) was used as an industry standard antimicrobial.

2.2. Bacteria cultures

The cultures of *D. desulfuricans* ATCC 27774 and *D. alaskensis* AL1 that served as inoculums for the "once-through" flow loop were grown in modified VMNI sulfate culture media [36]. VMN was composed of (g L^{-1} distilled water): NaCl, 20.0; NH_4Cl, 1.0; $CaCl_2 \times 2H_2O$, 0.04; Na_2SO_4, 4.5; $MgSO_4 \times 7H_2O$, 0.06; $FeSO_4 \times 7H_2O$, 0.004; sodium lactate, 6.0; KH_2PO_4, 0.5; sodium citrate, 0.3; casamino acids, 2.0; tryptone, 2.0; modified Wolfe's mineral elixir (0.1 (v/v) %) and vitamin solution (0.2 (v/v) %). The vitamin solution was composed of (g L^{-1} distilled water): riboflavin, 0.1; nicotinic acid, 0.25; thiamine, 0.3; pentatonic acid, 0.3; pyridoxine, 0.3; cyanocobalamin, 0.025; ascorbic acid, 1; biotin, 0.005. The composition of the modified

Wolfe's elixir was (g L^{-1} distilled water): Nitrilotriacetic acid, 1,5; $MgSO_4 \times 7H_2O$, 0.06; $MnSO_4 \times H_2O$, 0.5; NaCl, 1; $FeSO_4 \times 7H_2O$, 0.1; $CoSO_4 \times 7H_2O$, 0.1; $NiCl_2 \times 6H_2O$, 0.1; $CuCl_2 \times 2H_2O$, 0.1; $ZnSO_4 \times 7H_2O$, 0.1; $CuSO_4 \times 5H_2O$, 0.01; $AlK(SO_4)_2 \times 12H_2O$, 0.01; H_3BO_3, 0.01; $Na_2MoO_4 \times 2H_2O$, 0.01; $Na_2SeO_3 \times 5H_2O$, 0.001.

Cell densities of prepared enrichments were determinated using Thoma counting chamber (Helber Bacteria Cell, Hawksley, UK) with precondition that only viable cells are counted.

Flow cell A was inoculated two times with 80 mL and one time with 120 mL of *D. alaskensis* AL1 culture (cell densities≈10^7) and flow cell D with *D. desulfuricans* ATCC 27774 (cell densities≈10^7).

2.3. Analytical methods

2.3.1. Bacterial activity monitoring

Bacteria consortium monitoring in second bioreactor (indigent population naturally contained in seawater) and both flow cells (indigent population naturally contained in seawater + inoculated pure culture that are dominant) was conducted by measuring cell density. Firstly, global measurements were performed using a Thoma counting chamber with precondition that only viable cells are counted. Secondly, determination of cell densities for two groups (APB and SRB) was conducted using the most probable number (MPN) technique. Two types of media were used for these measurements: the full name acid producing bacteria (APB) media containing phenol red dye (APB, 25000 TDS) (Intertek Commercial Microbiology, USA) for APBs and Sulfate Reducing Bacteria (SRB) media 2 Medium (SRB, 25000 TDS) (Intertek Commercial Microbiology, USA) for SRBs. Measurements were performed 24 h after inoculations; samples were collected at the moment when flow conditions were reestablished.

2.3.2. Experimental media chemistry monitoring

Sulfate (SO_4^{2-}) concentrations were determinated spectrophotometrically with Spectroquant® sulfide kit (VWR, USA). Sulfide concentrations were monitored according to NACE TM0284-2003 (Appendix C—Determination of H_2S concentration) by the iodometric titration. Measurements were performed 24 h after inoculations, i.e. samples were collected at the moment when flow conditions were reestablished.

2.3.3. Electrochemical methods

Open circuit potential (OCP), linear polarization resistance (LPR) and electrochemical noise (EN) measurements were carried out using a multichannel potentiostat MultEchem™ (Gamry Instruments, USA) that consisted of two Reference 600TM Potentiostat/Galvanostat/ZRA independent units connected to a PC interface and monitored with DC105 or ESA410 software (Gamry Instruments, USA).

Standard three electrode-arrangements included a working electrode (WE), a counter electrode (CE) and a saturated calomel electrode (SCE). The WEs, made of S235JR low carbon steel, have a circular exposed area of 0.785 cm^2 (1 cm diameter cylindrical specimens, 2 cm long, dressed in polyolefin sleeve, Fig. 3).

The carbon steel specimens were manufactured from S235JR carbon (Descoure and Cabaud, France) whose composition is the following (mass ratio): 0.17% C, 1.4% Mn, 0.045% Cu, 0.03% S, and 0.03% P. Surfaces of all exposed steel specimens were prepared by manual grinding using increasing series of fine SiC paper, ending with 600-grit. Grinding debris was rinsed from the surface with sterile deionized water. The specimens were sterilized exposing them on each side for 12 h under UV light (wave length 256 nm: XX-15, sterilization UV lamp, UVP, USA) at 25 °C.

The CEs are made from Inconel® C276 cylindrical specimens (1 cm long, 1 cm diameter) with an exposed area of 3.95 cm^2 (flat circular face plus the side area).

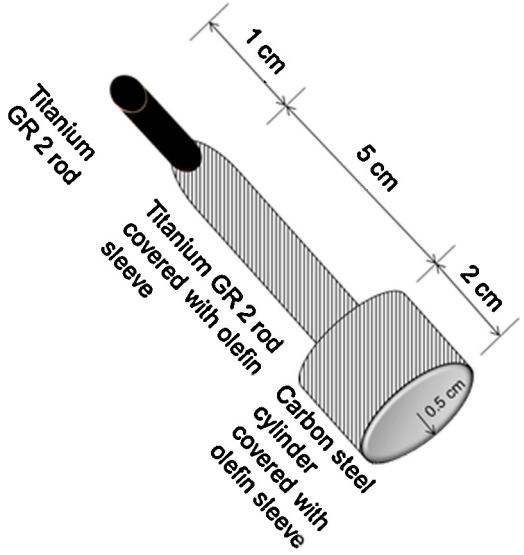

Fig. 3. Working electrode scheme.

In each flow cell, the OCP's versus SCE (E(OCP)/V (vs. SCE)) (SCE installed at F4 position) of six working electrodes (circular disc) installed at the F1, F2, F5, F8, F11 and F12 positions were recorded every 24 h in period prior and after flow cells perturbations (inoculations or antimicrobial treatments) or every 168 h during rest of test duration. Average OCP values with standard deviation error bars are reported.

The LPR technique was employed to estimate the corrosion rate of the steel coupons. The polarization resistance (R_p) of the steel/electrolyte interface is measured in the vicinity of the E(OCP)/V (vs. SCE) [37]. R_p is defined as the slope of the polarization curve tangent at the OCP. The inverse of R_p is proportional to the "instantaneous" corrosion rate and given in $1/\Omega$ [32]. To determine R_p, the potential was scanned in the range of E(OCP)/mV (vs. SCE) ± 10 mV with a sweeping rate of $v = 0.167$ mV s^{-1}. Polarization scans were performed every 24 h in period around flow cell perturbations (inoculations or antimicrobial treatments), or every 168 h during rest of test duration. Average $1/(R_p/\Omega)$ values with associated standard deviations were reported for the six different WEs installed at the F1, F2, F5, F8, F11 and F12 positions in each flow cell. Two counter electrodes (position F3 and F9) together connected at the potentiostat were used.

Electrochemical noise (EN) analysis was carried out to determine the type of corrosion attack [28]. Electrochemical current noise (ECN) and Electrochemical potential noise (EPN) signals were performed on four different three-electrode set-ups:

(1) WE1 at F1, WE2 at F2 and SCE at F4;
(2) WE1 at F7, WE2 at F8 and SCE at F4;
(3) WE1 at F5, WE2 at F6 and SCE at F4;
(4) WE1 at F11, WE2 at F12 and SCE at F4.

EN signals were recorded with frequency of 1 Hz, for 30 and 60 min long intervals, every 168 h during the whole test period. EN signals were recorded with a current range of 60 μA and a resolution of 1 pA and a potential range of ±30 mV and a voltage resolution of 1 μV. Only typical ECN signals characteristic for each experimental stage are presented herein. Modulated current signal patterns, as well as transients, characteristic of localized surface events, were visually examined within data blocks of 1000 or 10,000 (1 Hz sampling frequency) points resulting with the time resolution of 1000 or 10,000 s. The trend was removed from obtained data series by using the linear regression fitting method. The only ECN data are

presented herein, while accompanied EPN data are not presented in order to keep clarity of presented data even though EPN data support observed current transients.

2.3.4. Surface analysis

The morphology and chemical composition of formed surface deposits as well as steel surface topography were investigated using four different systems:

(1) High resolution Scanning Electron Microscope (SEM) JSM-7400F (Joel, Japan);
(2) Low vacuum table SEM TM3000 (Hitachi, Japan) interfaced with Energy Dispersive X-ray (EDX) spectroscopy system Quantax 70 (Bruker, USA);
(3) SEM Neon 40 EsB (Zeiss, Germany) equipped with a Inca EDX-System (Oxford Instruments, UK);
(4) Leica upright DMR microscope (Leica Microsystems GmbH, Germany) with attached ProgRes® C5 camera (JENOPTIK Optical Systems GmbH, Germany).

Two types of surface preparation were used depending on investigated specimen:

(1) In order to fix the biofilm/corrosion products layer, the steel specimens were placed in 2.5 (w/v) % glutaraldehyde (Electron Microscopy Science, USA) for 90 min at 4 °C, and then washed by four 15 min immersions in 0.1 M sodium cacodylate buffer (Merck, Germany). Post-fixation was carried out by placing specimens for 1 h in the solution of 1 (w/v) % osmium tetroxide (purity >99.95%, Electron Microscopy Science, USA) in 0.1 M sodium cacodylate buffer (MERCK, Germany). Post-fixed samples were washed in 0.1 M sodium cacodylate buffer (2 × 20 min) and dehydrated performing the following immersions: 15 min in 30 (v/v) %, 15 min in 50 (v/v) %, 20 min in 70 (v/v) %, 2 × 15 min in 96 (v/v) % and 2 × 15 min in 99.8 (v/v) % aqueous ethanol solutions (Sigma-Aldrich, Norway). De-watered specimens were placed in an oven (Type TS 4057, Thermaks AS, Norway) at 37 °C overnight. Dried samples were mounted on an aluminum stub using adhesive carbon tape, sputter-coated with gold for 3 min;
(2) Steel specimens were rinsed in deionized water to remove loose deposits.

After SEM/EDX examination, steel specimens were cleaned from surface deposits by following one of two used protocols:

(1) Immersion in a 5 (v/w) % hexamine (Merck, Germany) solution in concentrated HCl (VWR, USA) for 30 s. This was immediately followed by rinsing with deionized water, gentle blotting with a paper towel, and overnight storage in a desiccator;
(2) Immersion in AP2 solution (g L^{-1} of distilled water: 200, NaOH; 30, $KMnO_4$). This was immediately followed by rinsing with deionized water, gentle blotting with a paper towel, and overnight storage in a desiccator;

Finally, particular specimens were subjected to cross-section and microstructure examination. Etching was performed using standard Nital-etching solution (10 (v/v) % HNO_3 in ethanol).

Moreover, the presence of sulfide in black corrosion products on steel specimens, either retrieved from flow cells after 1070 or 2200 h of test, was tested by initiating reaction between concentrated HCl (VWR, USA) and collected corrosion products. Reaction product was H_2S, characterized by distinguish and easily recognizable smell [22].

3. Results and discussion

3.1. Development of event during test duration

To simplify the presentation and the consequent analyses of the test data, the current laboratory investigation was conveniently divided in three distinctive stages:

(1) First test stage refers to the period before the multiple inoculations of flow cells with pure SRBs cultures; from t_e = 0 h to t_e = 792 h.
(2) Second test stage covers the period from the first inoculation to first antimicrobial treatment; from t_e = 936 h to t_e = 1075 h.
(3) Third test stage comprises the period between the first antimicrobial treatment and test termination; from t_e = 1075 h to t_e = 2200 h.

As a general note concerning the bulk test medium, dissolved oxygen (DO) concentration and pH evolution monitored during the 2200 h of the test are shown in Fig. 4. According to the oxygen concentration evolution, the test environments were regarded as anoxic since the DO level was never above 50 ppb (0.049 mg L^{-1}).

3.1.1. First test stage

During the first test stage, pH around 8.1 (Fig. 4), low cell density (<10^3 cells mL^{-1}), corresponding to indigene population naturally present in seawater, high sulfate (≈3.5×10^3 ppm, i.e. 2.7 g L^{-1}), and low sulfide (not detectable) concentrations were detected in the bulk medium flowing through the both flow cells (Tables 1 and 2). It is then possible to conclude that the bulk medium conditions, exhibited in the two different flow cells, are very similar as expected (identical medium was flowing through both flow cells) proving that the further differences found could be attributed to the nature of the inoculations.

Measured instantaneous corrosion rates for WEs exposed in flow cells, obtained during the first test stage, are presented in Fig. 5. In both flow cells, $1/(R_p/\Omega)$ values measured during initial 200 h of tests were low, around 3×10^{-4}. After t_e = 200 h, $1/(R_p/\Omega)$ values decreased to 1×10^{-4}, where they remained (with some fluctuations) until end of the first test stage. Typical ECN records for WEs exposed in flow cells, obtained during the first test stage, and are presented in Fig. 6. ECN transients are oriented in both directions (up and down), indicating that both WEs are equally subjected to corrosion. This type of signal modulations is characteristic for the carbon steel immersed in chloride solution as seawater [38]. Moreover the magnitude of the ECN first increased with the time, as indicated by comparing the curves obtained for t_e = 20 h and for t_e = 200 h. Since the ECN is produced by independent current sources on steel surfaces [39], higher current reveals greater electrochemical activity and more pronounced anodic reaction being indicative for elevated corrosion rates [21,39]. Consequently in the test conditions, the initial increase of ECN magnitude can be explained by the breakdown of the initial protective ferrous layer, exposing bare steel surface to high amount of aggressive Cl^- ions present in seawater what may result in metastable pitting attacks. Afterward, since the tendency in corrosion rate showed a lessening ($1/(R_p/\Omega)$ plateau with lowest value in Fig. 5), ECN amplitudes decreased (Fig. 6, curves obtained at t_e = 400 h), indicating lower corrosion and lower surface activity. Theoretically, a protective layer of corrosion products, e.g. sulfated green rust ($GR(SO_4^{2-}) = Fe^{II}_4Fe^{III}_2(OH)_{12}SO_4 \times 8H_2O$), produced directly or by oxidation of iron hydroxide ($Fe(OH)_2$), is often found on the carbon steel surface when exposed to environments as described here [40–42]. Moreover, if any oxygen is present, certain portion of $GR(SO_4^{2-})$ will be oxidized into Fe(III)oxyhydroxides such as goethite (α-FeOOH) and lepidocrocite (γ-FeOOH) [40] (please note

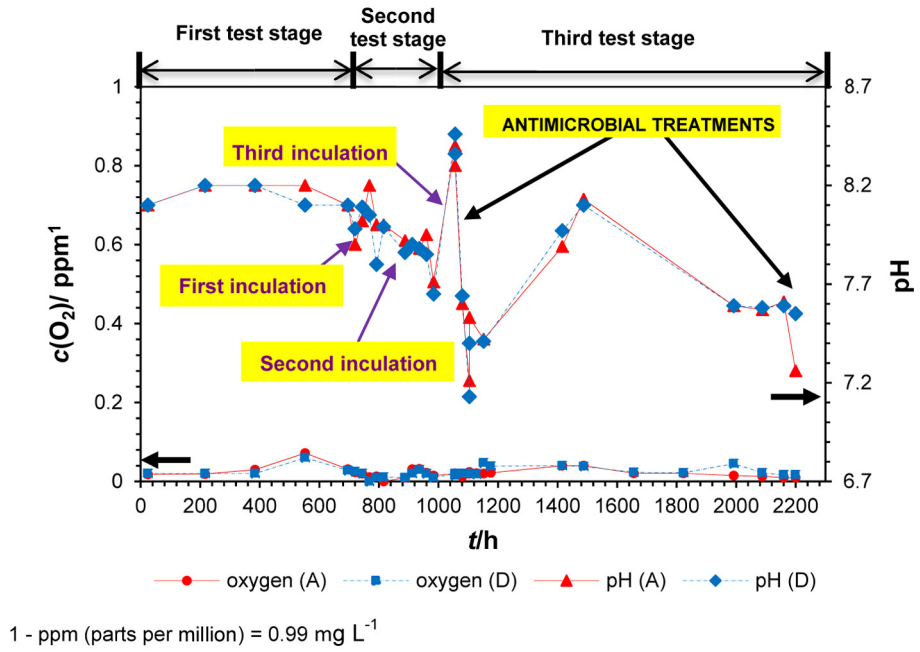

Fig. 4. Oxygen concentration in parts per million ($c(O_2)$/ppm) and pH evolution of bulk media in flow cell A (inoculation with *Desulfovibrio alaskensis*) and flow cell D (inoculation with *Desulfovibrio desulfuricans*) during the whole test.

that some oxygen is present in our system, Fig. 4). Interestingly, GR(SO_4^{2-}) may also serve as a source of sulfate, a terminate electron acceptor in SRBs dissimilatory respiration [40].

3.1.2. Second test stage

The first inoculation at the beginning of the second test stage (t_e = 792 h) led to an increase of cell density, a decrease in sulfate concentration linked to an increase in sulfide concentration due to the enhanced sulfidogenic metabolic processes (Tables 1 and 2).

However, no significant modifications were observed in the electrochemical response after this first inoculation: $1/(R_p/\Omega)$ remained stable with low values (Fig. 5). This stable trend in corrosion currents could be attributed to the corrosion product layer that remained stable even with the perturbation of the medium. In addition, sulfidogenic bacteria could enhance protective layer properties by promoting formation of protective iron sulfide (Fe_xS_y) films, a process taking place in a presence of low ferrous ion concentrations [43] as it is the case here. When flow conditions were reestablished, a decrease of the planktonic cell density in the bulk media was also observed in the both flow cells since part of microbial cells was flushed out. On the contrary, there was no change in sulfide and sulfate concentrations. Most likely the microbial activity in the bulk medium was maintained thanks to SRBs attached on steels surfaces that can detach and colonize the bulk medium.

The second inoculation imposed significant perturbation to the systems and resulted in a noticeable alteration of environment and material corrosion behavior. High cells densities were measured in both flow cells (Tables 1 and 2) even when the flux conditions were reestablished: Moreover higher densities were found in flow cell A (inoculated by *D. alaskensis*) than in the D one (inoculated by *D. desulfuricans*) with, respectively, 600 and 1850×10^3 cells mL^{-1}. A pH decrease down to 7.6 was noticed (Fig. 4) that

Table 1
Cell density and chemical monitoring of the bulk medium in flow cell A (inoculation with *Desulfovibrio alaskensis*) during whole test.

Time (h)	Cell density × 10^3 (cells mL^{-1})	APB × 10^3 (cells mL^{-1})	SRB × 10^3 (cells mL^{-1})	$c(SO_4^{2-}) \times 10^3$ (ppm)[a]	$c(S^{2-})$ (ppm)[a]	
First test stage						
336	1<	/	/	3.40	/	
672	1<	/	/	3.58	/	
Second test stage						
792	1<	/	/	3.15	/	First inoculation
816	555	/	/	3.00	34	
888	550	/	/	3.00	34	
936	39	/	/	2.95	37	Second inoculation
960	611	>140	>140	2.60	204	
1056	47	/	/	2.45	/	Third inoculation
Third test stage						
1070	678	/	/	2.40	206	First antimicrobial treatment
1094	506	/	/	3.15	136	
1152	468	>140	14	2.80	51	
1416	363	>140	>140	2.95	/	
1992	86	14	14	2.65	12	
2088	226	>140	45	2.45	5	
2180	/	/	/	/	/	Second antimicrobial treatment
2200	/	0.3	0.9	2.30	/	

[a] ppm = parts per million = 0.99 mg L^{-1}.

Table 2
Cell density and chemical monitoring of the bulk medium in flow cell D (inoculation with *Desulfovibrio desulfuricans*) during whole test.

Time (h)	cell density × 10^3 (cells mL^{-1})	APB × 10^3 (cells mL^{-1})	SRB × 10^3 (cells mL^{-1})	c(SO_4^{2-}) × 10^3 (ppm)[a]	c(S^{2-}) (ppm)[a]	
First test stage						
336	1<	/	/	3.40	/	
672	1<	/	/	3.58	/	
Second test stage						
792	1<	/	/	3.25	/	First inoculation
816	141	/	/	3.20	34	
888	109	/	/	3.20	34	
936	12	/	/	3.18	17	Second inoculation
960	1850	>140	>140	2.15	238	
1056	55	/	/	2.55		Third inoculation
Third test stage						
1070	1600	/	/	2.50	202	First antimicrobial treatment
1094	945	/	/	3.30	34	
1152	429	14	14	2.75	17	
1416	128	25	>140	2.75	/	
1992	70	1	1.4	2.25	20	
2088	166	140	9.5	2.50	20	
2180	/	/	/	/	/	Second antimicrobial treatment
2200	/	0.3	0.2	2.20	/	

[a] ppm = parts per million = 0.99 mg L^{-1}.

could be product of SRBs metabolic activity (souring due to elevated sulfide production). Side effect of observed microbial flourishing was a significant increase in instantaneous corrosion rate. It can be observed that 24 h after the second inoculation, the stable and low $1/(R_p/\Omega)$ plateau established during the first test stage was disturbed. This was displayed in a significant increase of the average $1/(R_p/\Omega)$ values up to 6×10^{-4} in the flow cell D, and less expressed increase up to 3.5×10^{-4} in the flow cell A, (Fig. 5), that can be correlated with the increase in cell density and metabolic activity (Tables 1 and 2). Also, ECN exhibited higher magnitude of corrosion current fluctuations and clear transients, characteristic of stable localized corrosion (i.e. pitting) as shown on Fig. 7. The stable localized corrosion was featured by significant current drops (I/nA = 100–500) followed by a slower increase. Briefly, the rapid current increase during pit initiation and growth is followed by a slower decay leading to pit repassivation [38]. It is possible to assume that second inoculation led to a breach threshold of the protective corrosion product layer. This layer managed to resist to the microbial activity introduced by the first inoculation but after the second inoculation, it suffered local breakdown and could not reestablish instantaneously, exposing localized areas of metal surface to different influences of e.g. aggressive ions such as Cl^-, S^{2-} and $S_2O_3^{2-}$, bacteria metabolic products. This often results in formation of large cathodic areas (remained Fe_xS_y, most likely with FeS) whereas significantly smaller unprotected regions of steel surfaces are forming anodes, characterized by higher anodic current. Besides, observed increase in corrosion, and therefore most likely increase in dissolved Fe concentration may have inhibited formation of a protective sulfide film on a steel specimens surfaces what could cause higher corrosion rates. This phenomenon has been previously observed by other researchers [44,45].

Short time after the third inoculation, a sudden pH increase was observed in the both flow cells (up to 8.5, Fig. 4), most probably due to cathodic corrosion reaction of hydrogen evolution and release of hydroxide ions (OH^-) into bulk medium, as a result of substantial increase in corrosion. This was reflected by the increase of the

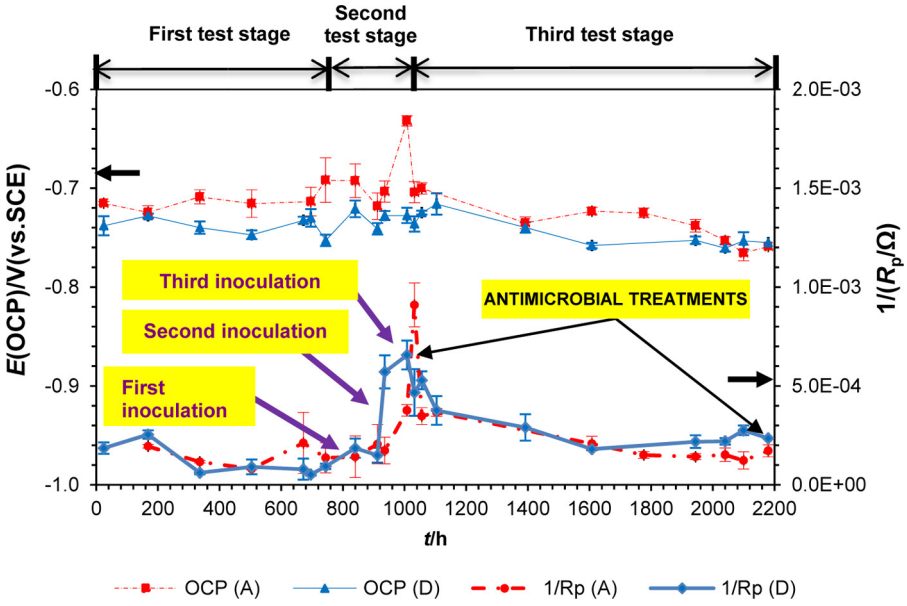

Fig. 5. Average instantaneous corrosion rate ($1/(R_p/\Omega)$) and OCP (E(OCP)/V (vs. SCE)) values with standard deviation error bars for 12 o'clock positioned steel specimens (WE) exposed in flow cell A (inoculation with *Desulfovibrio alaskensis*) and flow cell D (inoculation with *Desulfovibrio desulfuricans*) during the 2200 h of test.

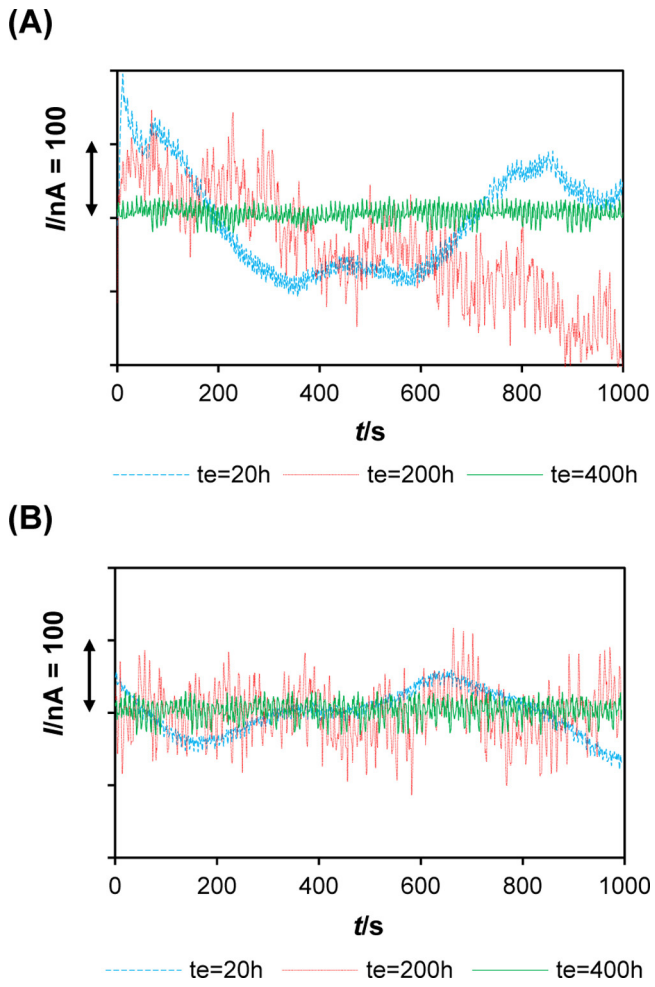

Fig. 6. Variations of typical current noise (I/nA = $f(t)$) obtained during the first test stage (t_e = 0–792 h, prior to inoculations) at t_e = 20 h, t_e = 200 h and t_e = 400 h: (A) in flow cell D (inoculation with *Desulfovibrio desulfuricans*); (B) in flow cell A (inoculation with *Desulfovibrio alaskensis*). Data linearly detrended.

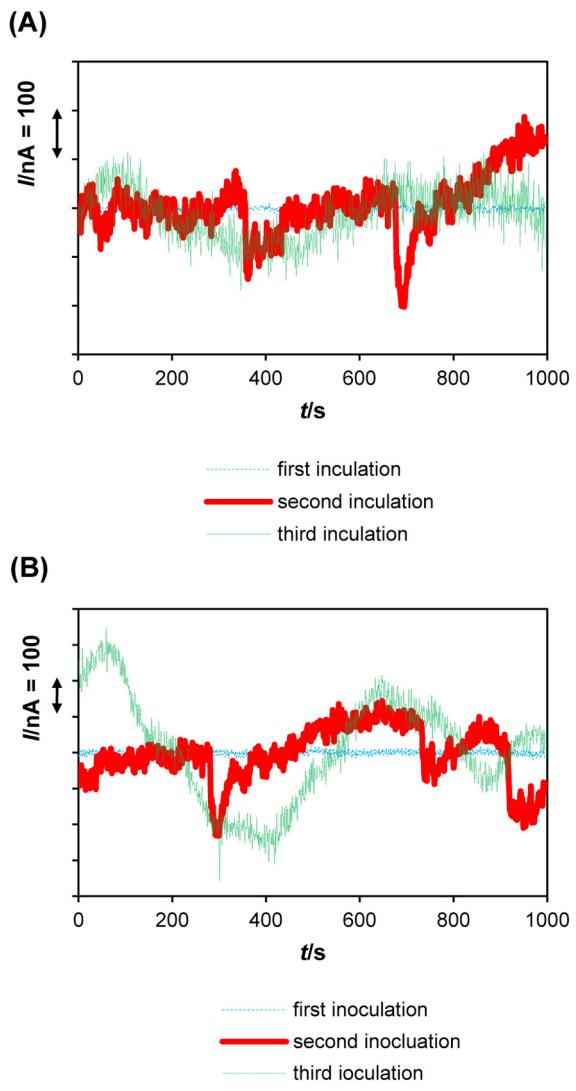

Fig. 7. Variations of typical current noise (I/nA = $f(t)$) obtained during the second test stage (t_e = 792–1070 h) obtained 24 h after each inoculation: (A) in flow cell D(inoculation with *Desulfovibrio desulfuricans*); (B) in flow cell A (inoculation with *Desulfovibrio alaskensis*). Data linearly detrended.

average $1/(R_p/\Omega)$ values (up to 9×10^{-4} for flow cell A and 7×10^{-4} for flow cell D, Fig. 5), and of the ECN amplitudes (Fig. 7). However, the ECN did not exhibit the geometry characteristic for pitting. Nonetheless, metastable pitting or conjugation of multiple pits in visually detectable general corrosion pattern would not be revealed by EN signals and surface degradation still would have origin in localized corrosion.

Micrographs presented in Fig. 8A and B are typical for steel specimens located at 6 o'clock position and retrieved from each flow cell at the end of the second test stage.

The steel specimens were covered with blackish deposits in which Fe_xS_y participated (sulfide presence verified by the chemical test). Deposits were easily removed from steel specimens. This is in agreement with chemical and microbial information obtained during second test stage. Detection of blackish deposits containing sulfide suggests that postulated layer formed during the second test stage is predominantly composed of the Fe_xS_y, a new component formed on steel surface. However, it is required to keep on mind that observed layer may be heterogeneous and may contain other compounds, such as GR(SO_4^{2-}) and/or magnetite (Fe_3O_4), characteristic for steel specimens immersed in seawater with active sulfidogenic microbial population [40,41,46]. Furthermore, SEM micrographs revealed a high variety of corrosion/biomineralization products at the metal surface suggesting that more than one mineral is participating in the corrosion deposit architecture. This indicates that members of indigent microbial population naturally contained in seawater (for example *Clostridium* [18]), in addition to the inoculated SRBs, are contributing to biomineralization process occurring on steel surfaces. Proof of this is the APB presence in both flow cells (Tables 2 and 3).

Moreover, observed corrosion products seem to be similar in presence of *D. alaskensis* (Fig. 8A) or *D. desulfuricans* (Fig. 8B), featured with particulate aggregates. On both surface observed (from flow cell A in Fig. 8A and from flow cell D in Fig. 8B), some bacteria with the characteristic curved rod shape of *vibrio* species [47] were observed incorporated inside the mineral structure instead of formation purely organic biofilms. The *vibrio* shape bacteria occupied a small volume fraction as compared to the formed corrosion products and biomineralized structures. After specimen's chemical cleaning, optical microscopy revealed presence of numerous pits with a diameter up to 100 μm and an average depth of 5–10 μm as shown on Fig. 9. These pits could be correlated with ECN transients observed 24 h after second inoculation, and indication occurrence of pitting on WEs surfaces.

3.1.3 . *Third test stage*

At the beginning of the third test stage, 19 h after the third inoculation, flow cells were treated with 500 ppm of a glutaraldehyde

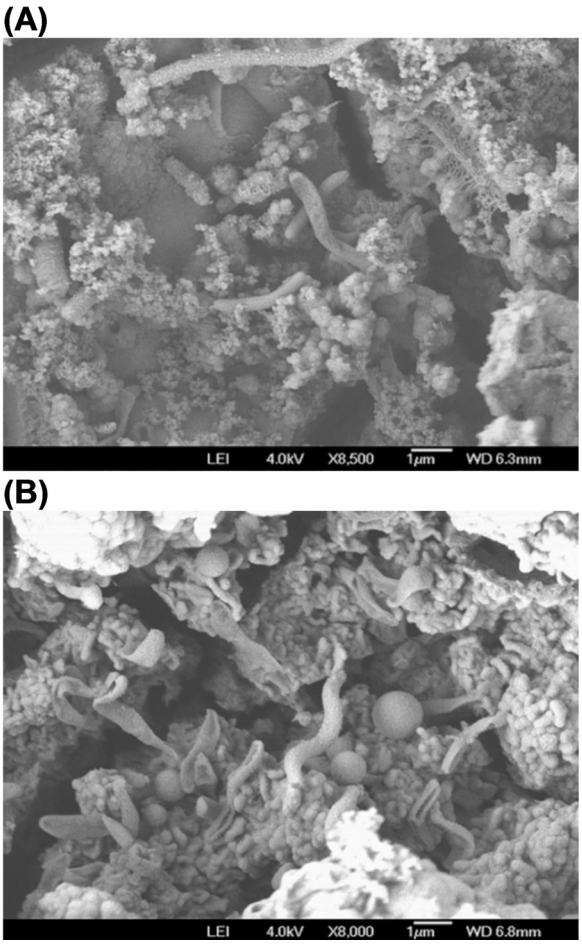

Fig. 8. SEM of steel specimens placed at 6 o'clock position and retrieved from flow cells after 1070 h of exposure: (A) specimen from cell A (inoculation with *Desulfovibrio alaskensis*)—8500×; (B) specimen from cell D (inoculation with *Desulfovibrio desulfuricans*)—8000×.

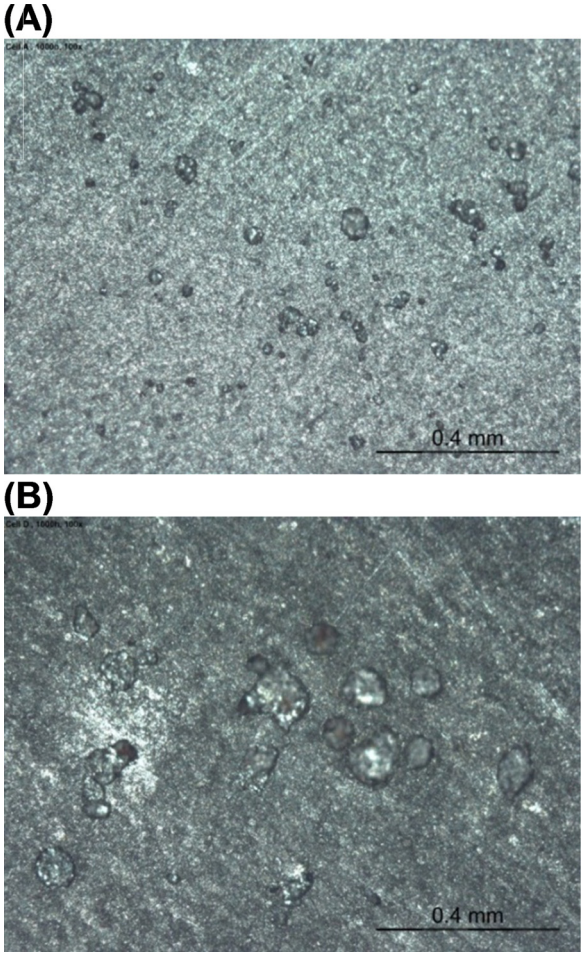

Fig. 9. Micro photographs (100×) of steel specimens retrieved from flow cells after 1070 h of exposure and after corrosion product removal, revealing localized corrosion attacks: (A) specimen from flow cell A (inoculation with *Desulfovibrio alaskensis*); (B) specimen from flow cell D (inoculation with *Desulfovibrio desulfuricans*).

based antimicrobial chemical for a period of 50 min (flow was stopped). Short time after the applied antimicrobial treatment, the pH decreased due to the intrinsic acidity of the antimicrobial chemical (Fig. 4). A decrease of cell densities was also observed, in a higher range in flow cell D (from 1600 to 945 cells mL^{-1} in few hours) than in the flow cell A (from 678 to 506 cells mL^{-1} in the same period). Consequently to this decrease, an increase of sulfate concentrations as well as a decrease of sulfide concentrations was measured indicating the effectiveness of the antimicrobial treatment. Moreover, $1/(R_p/\Omega)$ in both flow cells decreased to a value of 3.5×10^{-4} and recorded OCPs were E(OCP)/mV (vs. SCE)≈−720 (Fig. 5). Current fluctuations were found more expressed (Fig. 10) compared to those found before the antimicrobial treatment, maintaining

Table 3
EDX analysis results of emphasized areas presented on Fig. 13, all results given in weight fractions (wt(element)/%): (A) representative spectrums for Fig. 13A; (B) representative spectrums for Fig. 13B; (C) representative spectrums for Fig. 13C.

Table A					
Spec.[a]	C	O	S	Ca	Fe
Sp1	18.2	35.9	5.2	3.0	37.6
Sp2	30.5	11.7	5.0	3.5	49.3
Sp3	2.6	6.9	6.7	13.3	70.5
Table B					
Spec.[a]	C	O	S	Ca	Fe
Sp1	3.1	5.3	6.5	13.5	71.4
Sp2	20.0	40.2	3.9	3.2	32.9
Sp3	3.4	6.0	2.5	1.3	86.8
Table C					
Spec.[x]	C	O	S	Ca	Fe
Sp1	15.1	19.9	12.6	4.2	48.3
Sp2	25.5	37.1	6.9	1.4	29.1
Sp3	20.1	9.2	13.2	2.6	68.1

[a] Spec. = complete analyzed spectrum for particular surface area.

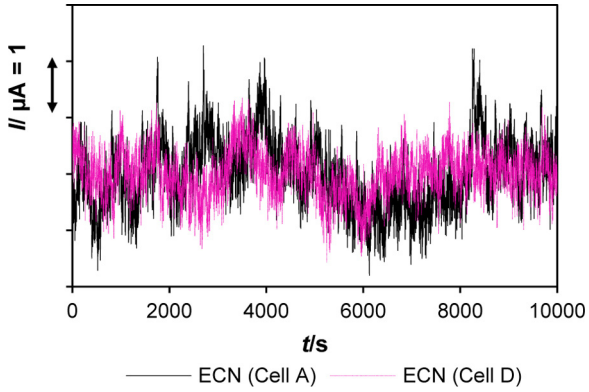

Fig. 10. Variations of typical current noise (I/nA = $f(t)$) obtained in flow cell A (inoculation with *Desulfovibrio alaskensis*) and flow cell D (inoculation with *Desulfovibrio desulfuricans*) recorded 12 h after first antimicrobial treatment (t_e = 1087 h). Data linearly detrended.

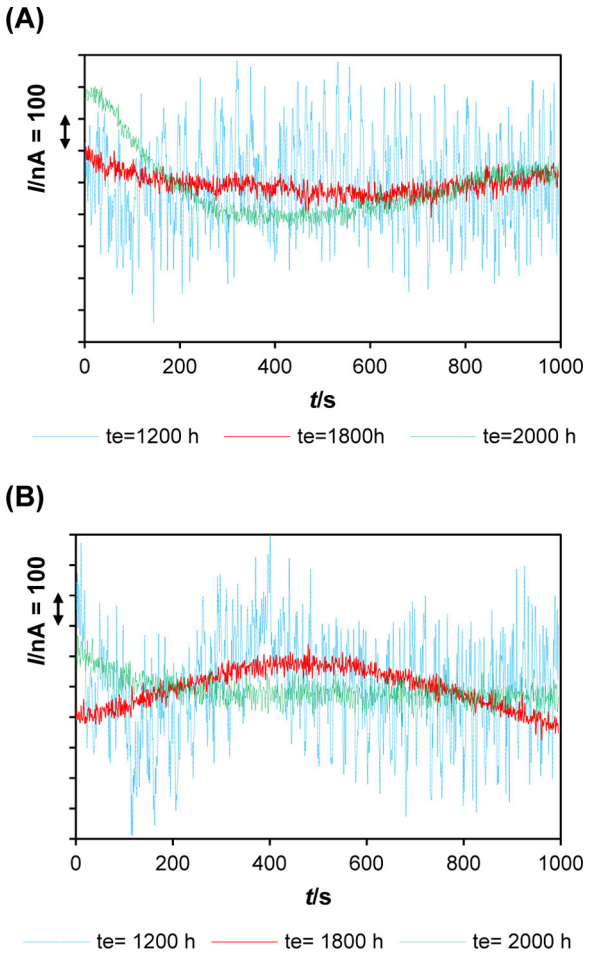

Fig. 11. Variations of typical current noise (I/nA = $f(t)$) obtained during the third test stage (t_e = 1070–2200 h) at t_e = 1200 h, t_e = 1800 h and t_e = 2180 h: (A) in flow cell D(inoculation with *Desulfovibrio desulfuricans*); (B) in flow cell A (inoculation with *Desulfovibrio alaskensis*). Data linearly detrended.

constantly differences between minimum and maximum amplitudes peaks in range of approximately 1 μA (versus 100 nA). Even though graphs are not presented herein, it is significant to mention that in this short period after biocide treatment (2–10 h), EPN trend rose toward more positive values, from E/mV (vs. SCE) = −720 up to E/mV (vs. SCE) = −680 and then returned back to E/mV (vs. SCE) = −720 in the both flow cells. When antimicrobial was flushed out from flow cells, pH showed increasing trend behavior due to

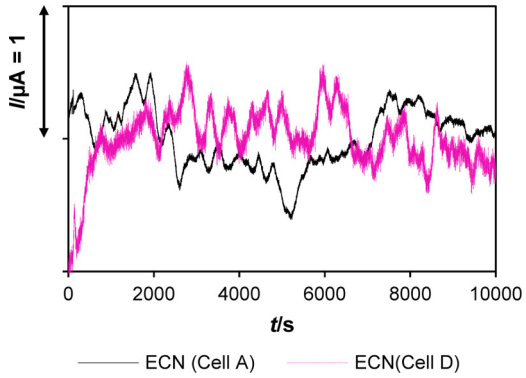

Fig. 12. Variations of typical current noise (I/nA = $f(t)$) obtained in flow cell A (inoculation with *Desulfovibrio alaskensis*) and flow cell D (inoculation with *Desulfovibrio desulfuricans*) recorded 12 h after the second antimicrobial treatment (t_e = 2192 h). Data linearly detrended.

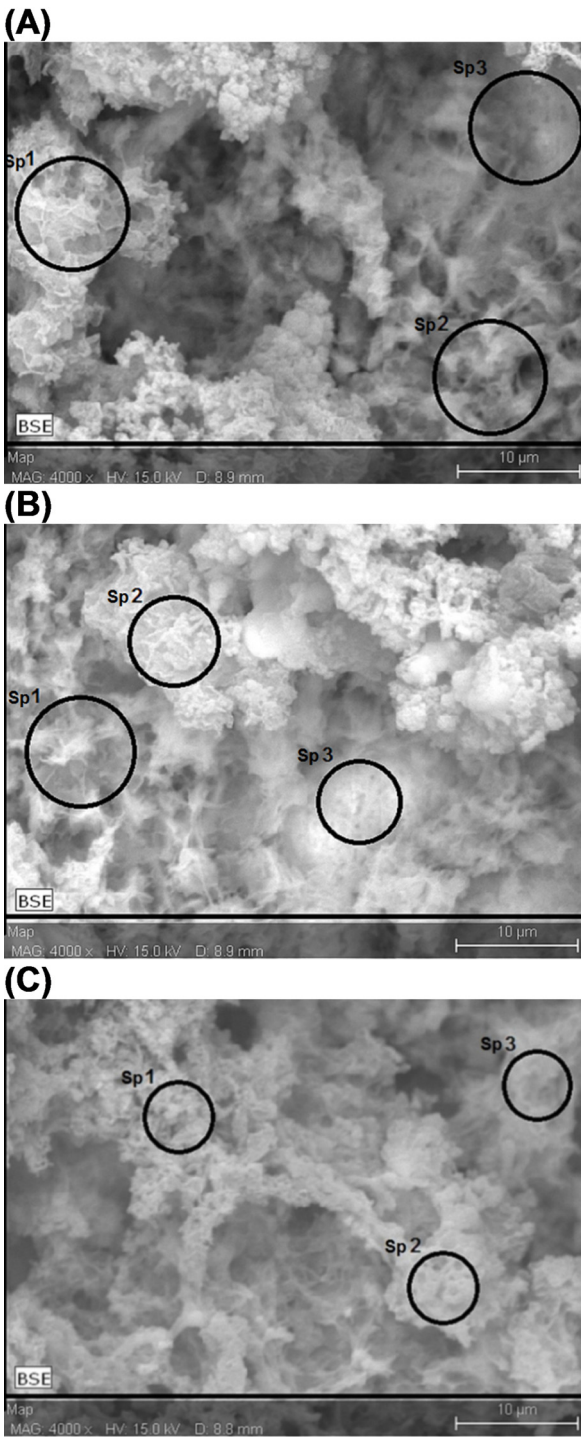

Fig. 13. SEM micrographs (4000×) with emphasized areas submitted to EDX analysis of four 6 o'clock positioned specimens exposed in flow cell A (inoculation with *Desulfovibrio alaskensis*) for 2200 h.

income of fresh media. This process was slow and it resulted in pH 8.1 at t_e = 1450 h (Fig. 4). From that point until the test termination, both flow cells exhibited a decrease in pH with final pH of 7.4 in flow cell A and 7.7 in flow cell D (Fig. 4).

Despite these fluctuations, measured pH was very similar to that of seawater from North Sea (base component of used media). During the same time period cell densities continued to slowly decrease (Tables 2 and 3). After a temporary increase initiated by the first antimicrobial treatment, sulfate concentration showed a decreasing trend during the whole third test stage (Tables 1 and 2).

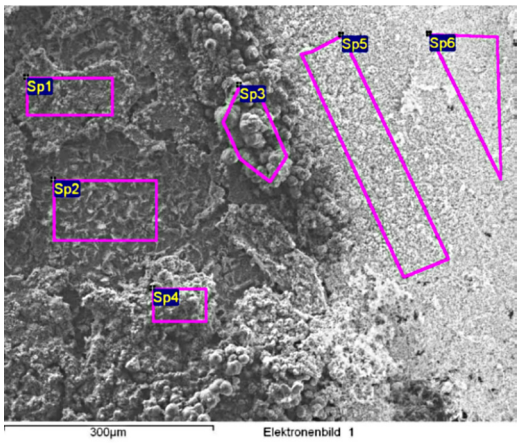

Fig. 14. SEM micrograph (100×) with emphasized areas submitted to EDX analysis of 12 o'clock positioned specimen exposed in flow cell A (inoculation with *Desulfovibrio alaskensis*) for 2200 h.

Acquired data are suggesting that bacteria continued to consume sulfate present in seawater; however, produced sulfide was found in low concentration in bulk medium (sulfide concentration continued to decrease). In fact, it reacted with iron forming different Fe_xS_y compounds that can be observed on steel specimens' surfaces as well as in bulk medium where black particulates were found. In addition, part of sulfate probably reacted with residual oxygen forming thiosulfate ions, and decreasing amount of available sulfate in bulk medium. Observed reduction in sulfate concentration will reduce the molar ratio $[SO_4^{2-}]/[HCO_3^-]$ and consequently lead to partial transformation of $GR(SO_4^{2-})$ to carbonated green rust ($GR(CO_3^{2-}) = Fe^{II}_4Fe^{III}_2(OH)_{12}CO_3 \times 2H_2O$) [42]. Moreover, possible increase of the carbonate concentration could result in the formation of carbonated compounds such as chukanovite ($Fe_2(OH)_2CO_3$) [48,49].

The $1/(R_p/\Omega)$ decreasing trend observed in both flow cells after antimicrobial treatment was reduced and material corrosion resistance stabilized to the initial level. This was maintained until test termination, and final $1/(R_p/\Omega)$ were around 2×10^{-4} (Fig. 5). OCPs exhibited similar behavior, featured with mildly decreasing OCPs and final value of E(OCP)/mV (vs. SCE) = −770 (Fig. 8). ECN signals acquired 125 h after biocide treatment (Fig. 11, t_e = 1200 h) exhibit lower amplitudes indicating decrease of surface electrochemical activity compared to ECN signals obtained shortly after antimicrobial treatment (Fig. 12). Later on, the low current fluctuations observed at t_e = 1800 h and t_e = 2000 h in the range of 100 nA (Fig. 11) indicated current intensity decrease, hence lower corrosion too. This is in agreement with observed decrease of $1/(R_p/\Omega)$ and reduced of the planktonic bacterial population. In conclusion, the probable formation of stable corrosion products and the partially suppressed microbial activity can be considered as the origin of the electrochemical behavior of carbon steel after the antimicrobial treatment.

The second antimicrobial treatment (50 min with 1500 ppm) completely suppressed already decreased planktonic microbial activity. Here again, the pH decreased as a consequence of applied treatment. As previously mentioned, E(OCP)/mV (vs. SCE) and $1/(R_p/\Omega)$ values in both cell remained unchanged. However, as observed immediately after the first biocide treatment, ECN exhibited particular alteration in its behavior (Fig. 12). The ECN in both cells demonstrated more erratic behavior compared to ones observed before antimicrobial treatment application. The observed curve shape and peak magnitude suggest elevated corrosion current and enhanced localized surface activity. These observations could indicate corrosion deposit breakdown, possibly initiated by pH decrease.

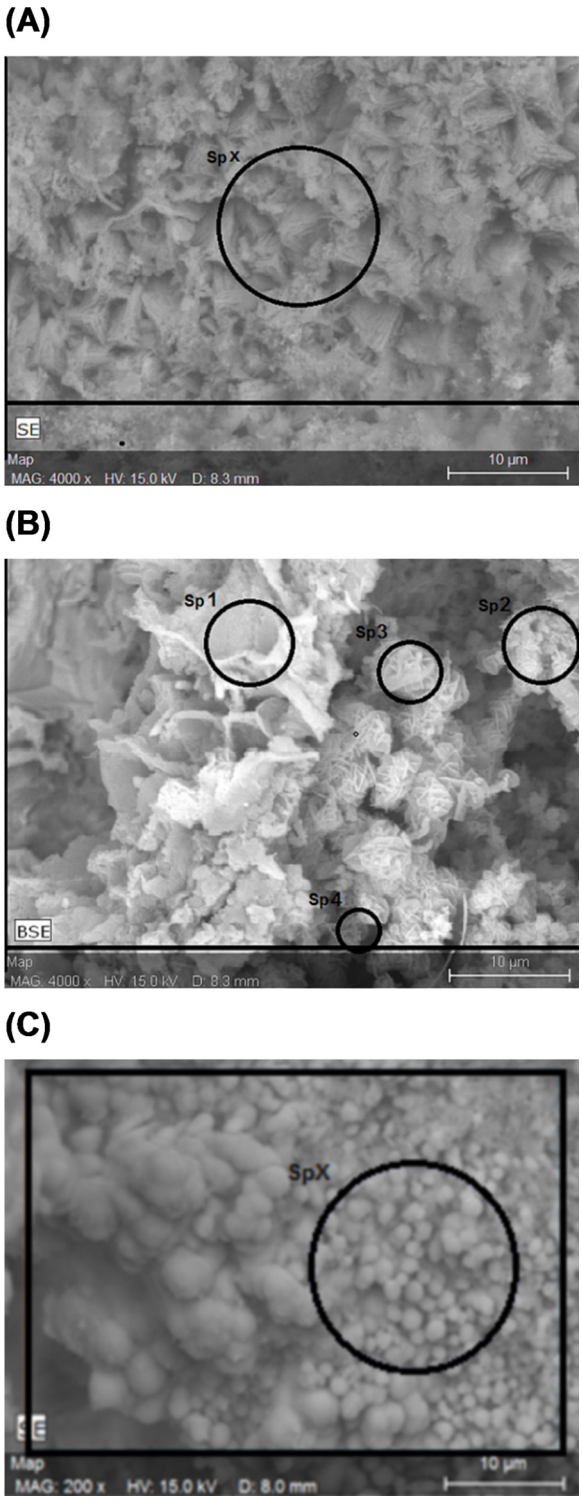

Fig. 15. SEM micrographs (4000×) with emphasized areas submitted to EDX analysis of three 6 o'clock positioned specimens exposed in cell D (inoculation with *Desulfovibrio desulfuricans*) for 2200 h.

3.2. Post- test surface analysis

After the once-through flow loop was decommissioned, three 6 o'clock positioned steel specimens and one 12 o'clock positioned steel specimen (WE) from each cell were subjected to microscopical

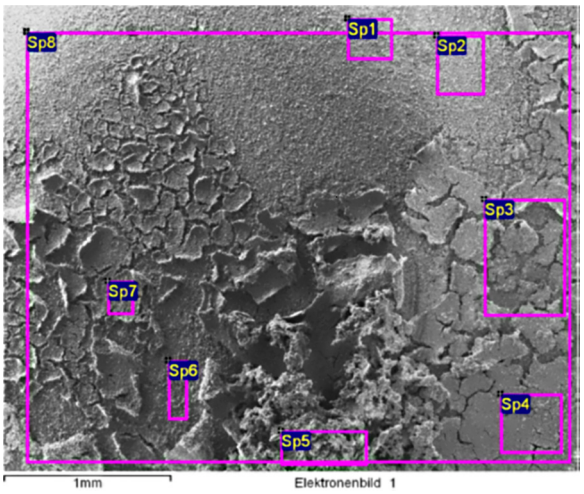

Fig. 16. SEM micrograph (100×) with emphasized areas submitted to EDX analysis of 12 o'clock positioned specimen exposed in flow cell D (inoculation with *Desulfovibrio desulfuricans*) for 2200 h.

(SEM analysis) and chemical (EDX analysis) examination in order to acquire more information about corrosion deposits building blocks and corrosion mechanisms nature.

3.2.1. Corrosion products architecture

The micrographs for 6 o'clock located steel specimens, examined with SEM/EDX system after 2200 h exposure in the flow cell A with a dominant presence of *D. alaskensis* species are presented in Fig. 13. Table 3 shows EDX analysis obtained on different points on the observed surface.

The micrographs reveal the deposition of corrosion products characterized with the dominant presence of Fe, Ca, S, C and O, but the proportions and amounts of specific elements are various, suggesting different mineral structures. Indeed, the simultaneous presence of Fe peak with O and C ones (spot Sp1 of Fig. 13A, Table 3A; spot Sp2 of Fig. 13B, Table 3B; spots Sp1 and Sp2 of Fig. 13C, Table 3C) is characteristic of the formation of iron minerals, such as $Fe_2(OH)_2CO_3$ and $GR(CO_3^{2-})$) [48,49]. These mineral products were found in outer corrosion product structure. Moreover, S peaks were identified with EDX analysis too. However, S was found in higher proportion at locations where analyses were performed close to the metal surface, as shown in Fig. 13A Sp3 (Table 3A), Fig. 13B Sp1 (Table 3B) and Fig. 13C Sp1, Sp2 and Sp3 (Table 3C). Concerning Ca peaks, analysis is suggesting that Ca was concentrated within localized and visually larger structures established in the outer layers of corrosion products, and often accompanied with the presence of O and C as shown in Fig. 13A Sp3 (Table 3A), and Fig. 13B Sp1 (Table 3B). The simultaneous presence of Ca, C and O with local alkaline surface conditions (as recorded at the end of second test stage) could indicate the formation of calcite ($CaCO_3$) [50]. To sum-up, taking into consideration relatively low DO in the bulk medium (Fig. 1), mildly alkaline environment (Fig. 4) and OCP in range of E(OCP)/mV (vs. SCE) = -750 ± 20 (Fig. 2), it is likely that the corrosion/biomineralization products belong to several main mineral families: iron sulfides with FeS, iron oxides with Fe_3O_4, iron(III) oxyhydroxides in all likelihood with α-FeOOH and γ-FeOOH, $GR(SO_4^{2-})$, carbonate minerals most likely with $Fe_2(OH)_2CO_3$ and $GR(CO_3^{2-})$, as well as calcareous such deposits as $CaCO_3$ on the top of this structure [42,49].

Otherwise, micrograph presented in Fig. 14 is characteristic for the 12 o'clock positioned WEs and removed from the flow cell A after 2200 h exposure. They reveal the presence of two dominant regions as corrosion deposits and transfer region defined by spot Sp3. Two dominant regions have similar chemical fingerprints to ones observed in a case of 6 o'clock positioned steel specimens. The first region, defined by spots Sp1, Sp2 and Sp4 on Fig. 14, is dark colored and EDX analysis emphasized the presence of S, as well as high portions of Fe, O and C (Table 4), suggesting presence of Fe_xS_y in high amount along with the presence of iron oxides and carbonate minerals. In contrast, the second zone, represented by spots Sp5 and Sp6 on Fig. 14, appears brighter compared to the dark region, is forming outer layer, and reveals high amount of Ca (Table 4). Additionally, Fe, O, and C are well represented; suggesting formation of

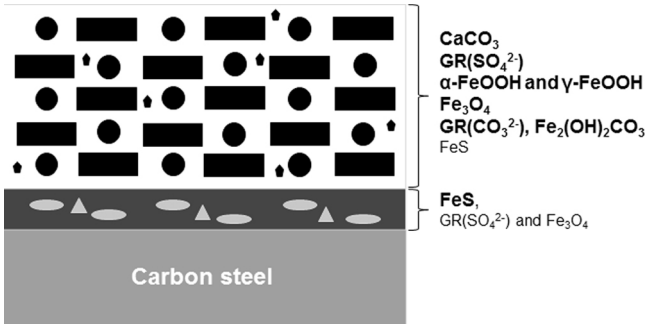

Fig. 17. Phenomenological model for corrosion products formed on the carbon steel surface during and post sulfidogenic bacteria process.

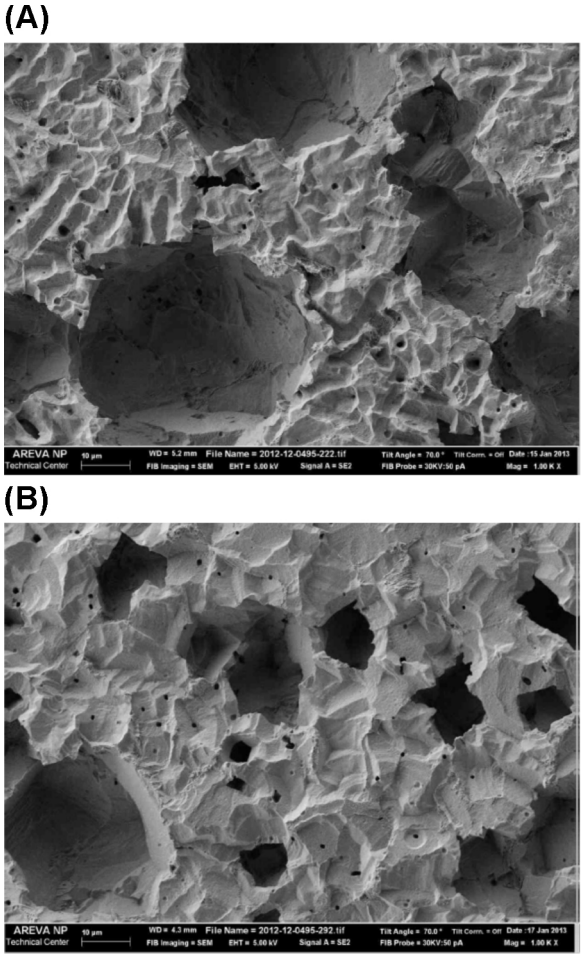

Fig. 18. SEM micrographs (1000×) of 12 o'clock positioned steel specimens retrieved after 2200 of immersion in flow cells and chemically cleaned from corrosion deposits: (A) specimen from flow cell A (inoculation with *Desulfovibrio alaskensis*); (B) specimen from flow cell D (inoculation with *Desulfovibrio desulfuricans*).

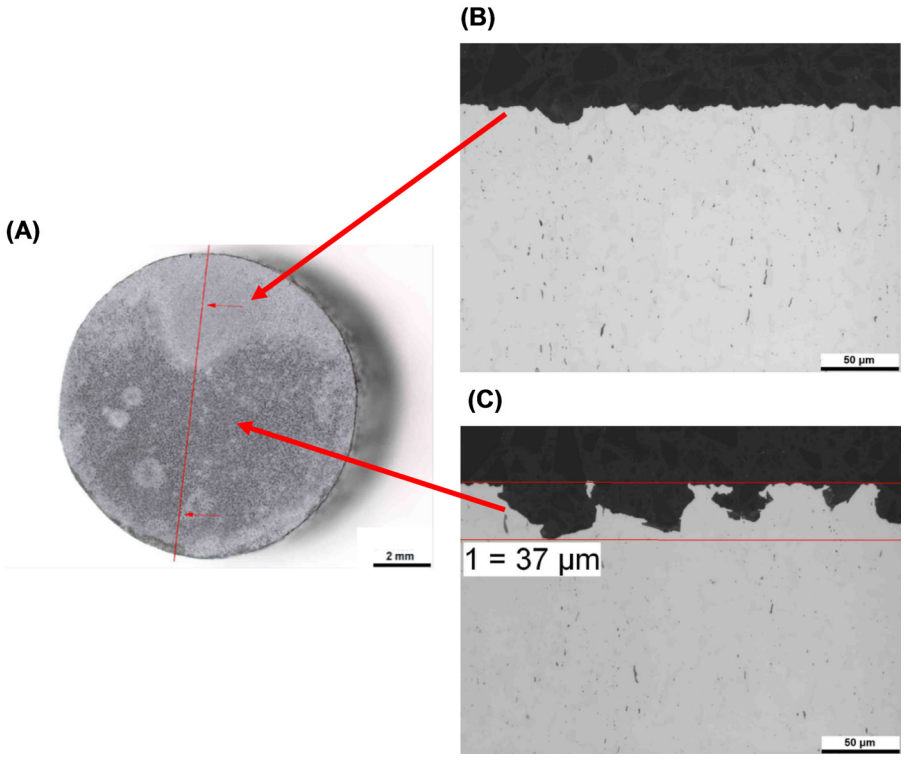

Fig. 19. Macrographs and micrographs of 12 o'clock positioned specimen exposed in cell A (inoculation with *Desulfovibrio alaskensis*) for 2200 h after corrosion product removal: (A) Macrograph before cross section and cutting line; (B) Micrograph for depth determination of attack in more lighted coloured region; (C) Micrograph for depth determination of attack in darker coloured region.

Table 4
EDX analysis results of emphasized areas presented on Fig. 14, all results given in weight fractions (wt(element)/%).

Spec.[a]	C	O	Na	Mg	Al	Si	P	S	Cl	Ca	Cr	Mn	Fe	Ni	Cu	Sr
Sp1	8.6	42.7	/	0.4	0.3	/	0.1	16.6	/	0.2	/	0.2	30.8	/	/	/
Sp2	6.5	34.7	/	0.2	0.4	0.2	0.4	7.9	0.6	/	1.1	1.2	42.0	1.1	3.8	/
Sp3	5.1	53.6	/	1.0	0.3	0.3	/	0.1	/	1.0	/	0.4	38.2	/	/	/
Sp4	12.5	36.7	0.8	1.4	0.2	0.2	/	17.8	/	1.4	/	/	28.9	/	/	/
Sp5	5.7	61.9	/	0.6	/	/	/	/	0.2	15.1	/	/	16.5	/	/	/
Sp6	10.6	57.8	0.3	0.1	0.1	/	/	0.1	0.1	27.1	/	/	3.3	/	/	0.5

[a] Spec. = complete analyzed spectrum for particular surface area.

iron oxides, iron carbonates and Ca-based minerals. Interesting to note for this particular region is the complete absence of S peak in investigated spectrums. To sum-up, micrographs suggest an initial formation of Fe_xS_y (inner layer) that is followed by the rise of different Fe minerals and Ca-based minerals on them (outer layer). However, this postulated layered structure may be not so obvious and some detected compounds may participate in construction of the both layers. Additionally, P peak was occasionally recorded (Sp1 and Sp2, Fig. 14) but overall impression differs a lot from observations made in artificial seawater systems inoculated with different SRB strains, *D. gabonensis* and *D. capillatus*, for which P was present in much larger amount accompanied with less S [14]. Moreover, Si, Al and Mg peaks were detected (Fig. 14, Table 4). The Mg, in the form of Mg(II), possibly could substitute Fe(II) in GR compounds but it can also easily substitute Ca in calcite.

Micrographs presented in Fig. 15 show corrosion products formed on steel specimens located at 6 o'clock location after 2200 h immersion in the dominant presence of *D. desulfuricans* species (flow cell D). It is possible to observe corrosion products composed of Ca-based minerals (Fig. 15A SpX, Table 5A), carbonate minerals (Fig. 15B Sp4 and Table 5B), and also some Fe_xS_y minerals (Fig. 15B Sp2, Sp3Sp4 and Table 5B). Moreover, a high amount of iron oxide minerals (Fig. 15C SpX, Table 5C) is present. It possesses

Table 5
EDX analysis results of emphasized areas presented on Fig. 15, all results given in weight fractions (wt(element)/%): (A) representative spectrums for Fig. 15A; (B) representative spectrums for Fig. 15B; (C) representative spectrums for Fig. 15C.

Table A						
Spec.[a]	C	O	S	Ca	Fe	Mg
SpX	15.2	45.0	1.3	26.6	5.2	1.8
Table B						
Spec.[a]	C	O	S	Ca	Fe	
Sp1	20.1	17.6	4.1	0.9	54.7	
Sp2	2.2	7.1	10.7	1.1	78.8	
Sp3	/	8.2	11.0	1.8	79.0	
Sp4	1.8	6.6	14.2	3.3	74.0	
Table C						
Spec.[a]	O	Fe				
SpX	10.0	90.0				

[a] Spec. = complete analyzed spectrum for particular surface area.

resemblance, in terms of morphology and analysis, with magnetite mineral.

Micrographs presented in Fig. 16 reveal the presence of relatively homogenous minerals morphologies as corrosion products on the 12 o'clock positioned WE examined with SEM/EDX system after 2200 h exposure in the flow cell D. The S is very well

Table 6
EDX analysis results of emphasized areas presented on Fig. 16, all results given in weight fractions (wt(element)/%).

Spec.[a]	C	O	Na	Mg	Al	Si	P	S	Cl	Ca	Cr	Mn	Fe	Ni	Cu	Zn
Sp1	12.3	47.6	1.2	1.2	0.4	0.2	0.4	4.6	0.4	/	0.4	0.6	28.4	0.8	1.5	/
Sp2	16.0	43.2	0.8	0.9	0.4	0.3	0.5	8.0	0.4	0.2	0.5	0.7	24.9	1.1	1.5	0.6
Sp3	14.2	54.7	0.3	0.9	0.4	/	0.1	11.8	0.5	0.6	0.2	0.2	16.2	/	/	/
Sp4	15.7	52.4	0.3	0.9	0.1	/	0.1	13.6	0.8	1.2	/	0.1	14.7	/	/	/
Sp5	19.6	49.8	0.5	1.1	1.2	/	/	9.9	0.3	7.3	/	/	10.4	/	/	/
Sp6	8.1	66.2	1.8	0.3	0.5	0.1	0.2	2.9	0.6	/	/	0.4	18.4	/	0.2	/
Sp7	23.6	55.1	0.2	1.5	0.2	/	0.2	9.3	0.4	0.7	/	/	8.8	/	/	/
Sp8	17.4	53.1	0.9	1.1	0.5	0.1	0.3	9.4	0.3	0.8	0.2	0.3	15.0	0.3	0.3	/

[a] Spec. = complete analyzed spectrum for particular surface area.

represented in corrosion deposits (Fig. 16 in Sp2, 3, 4, 5, 7 and 8; Table 6). Then again, Ca is well represented only in some part (spot Sp5 in Fig. 16, Table 6), regarded as the outer layer, indicating similar corrosion products architecture as previously described for the specimens removed from the flow cell A. This is equally supported by the presence of C and O that are quantitatively dominant compared to other elements discovered in this scan.

Taking all the observations into account, a phenomenological model of the architecture of the corrosion deposits formed in our particular test conditions, is suggested, regardless cells were inoculated with *D. alaskensis* or *D. desulfuricans* species (Fig. 17). As Fe_xS_y minerals seemed placed deeper, in the inner layers of corrosion product structure, it could correspond to the biological sulfate reduction into sulfide ions. Undeniably, *Desulfovibrio* species are anaerobic bacteria capable of reducing sulfur compounds to sulfide, what finally may result with growth of Fe_xS_y.

In our work, where experiments have been conducted under anoxic conditions in North Sea seawater, Fe_xS_y compounds seem to be the construction blocks of the first corrosion product layer which stays stable on the metal surface, even after a long time immersion in presence of elevated metabolic activity of SRBs. This layer may also contain GR(SO_4^{2-}) and Fe_3O_4. Then, above this first layer, mixed iron minerals (Fe_3O_4, Fe(III) oxyhydroxides such as α-FeOOH and γ-FeOOH, GR(SO_4^{2-}), $Fe_2(OH)_2CO_3$ and GR(CO_3^{2-})) with addition of calcareous precipitates ($CaCO_3$) are established. This layer possibly could contain small amounts of Fe_xS_y (most likely FeS) too. This structural environment (corrosion products, bacteria) seems to entail a localized corrosion process with the presence of pits on the steel surface.

3.2.2. Corrosion attack mechanism and evolution

In order to identify corrosion attack mechanisms and their evolution during the test time, steel specimens were cleaned of corrosion products/deposits and submitted to microscopical and metallurgical examination.

After corrosion products removal, the surface topography, representative of the 12 o'clock positioned WEs retrieved from both flow cells, appear very rough (Fig. 18) with numerous pits, with a diameter up to 50–60 μm for specimens retrieved from cell A (Fig. 18A) and 20–30 μm for specimens retrieved from cell D (Fig. 18B). Also, metallographic cross sections of same steel specimens were prepared in order to determine the depth and the characteristics of the corrosive attack (Figs. 19 and 20).

As previously mentioned (see Section 3.2.1), the corrosion deposits on the surface were subdivided in darker and brighter regions, even after the removal of corrosion products (19A and 20B). The darker zones are less spread on the specimens from the flow cell D (inoculated with *D. desulfuricans*). These different visual appearances correspond to different characteristics of attack in the metallographic cross section. The brighter areas are rather smooth, showing only a superficial attack (Fig. 19B) whereas higher roughness and pitting corrosion can be observed in the darker areas

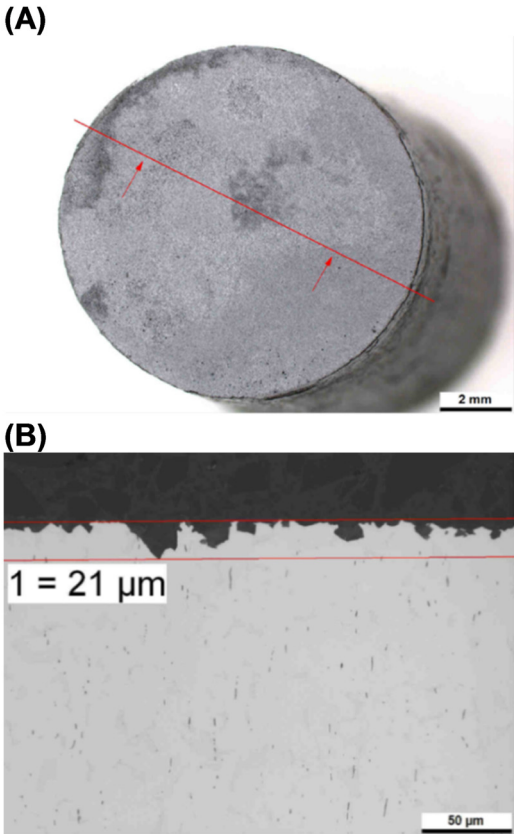

Fig. 20. Macrograph and micrograph of 12 o'clock positioned specimen exposed in cell D (inoculation with *Desulfovibrio desulfuricans*) for 2200 h after corrosion product removal: (A) Macrograph before cross section and cutting line; (B) Micrograph for depth determination of attack.

(Fig. 19C). While the depth of the corrosion attack varies between approximately 20 μm to 40 μm on the specimen from the flow cell A (inoculated with *D. alaskensis*, Fig. 19C), the degree of damage is lower regarding depth, in range of approximately 20 μm, on the specimen from the flow cell D (Fig. 20B), indicating lower material deterioration.

This is understandable, having on mind higher results suggesting that *D. alaskensis* has a higher corrosivity than *D. desulfuricans*. Regardless to size and depth of pits, the topographies observed here are coherent with corrosion attack previously recorded in presence of SRBs, supporting hypothesis that biofilms constituted of SRBs lead to pitting corrosion [33].

The bulk microstructure of all steel specimens used in this study consists of ferrite and pearlite with randomly distributed MnS inclusions, which is the typical microstructure of the material

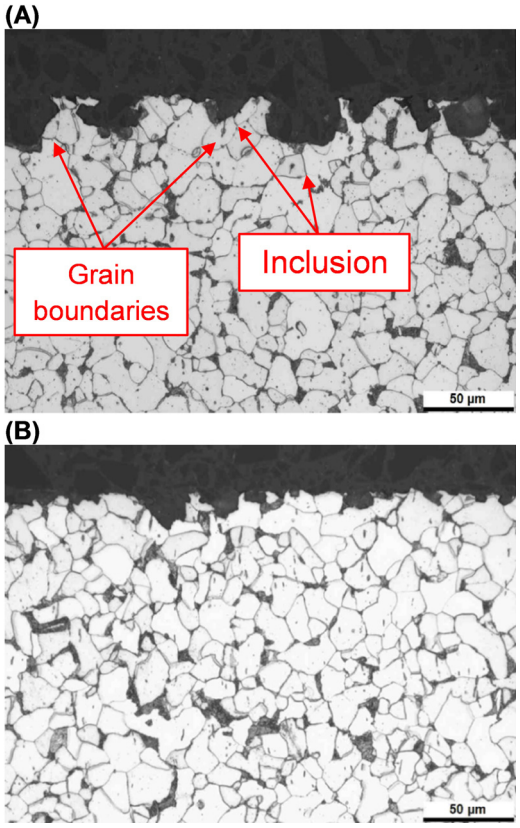

Fig. 21. Etched cross-sections SEM micrographs (250×) of 12 o'clock positioned specimen exposed for 2200 h: (A) from flow cell A (inoculation with *Desulfovibrio alaskensis*); (B) from flow cell D (inoculation with *Desulfovibrio desulfuricans*).

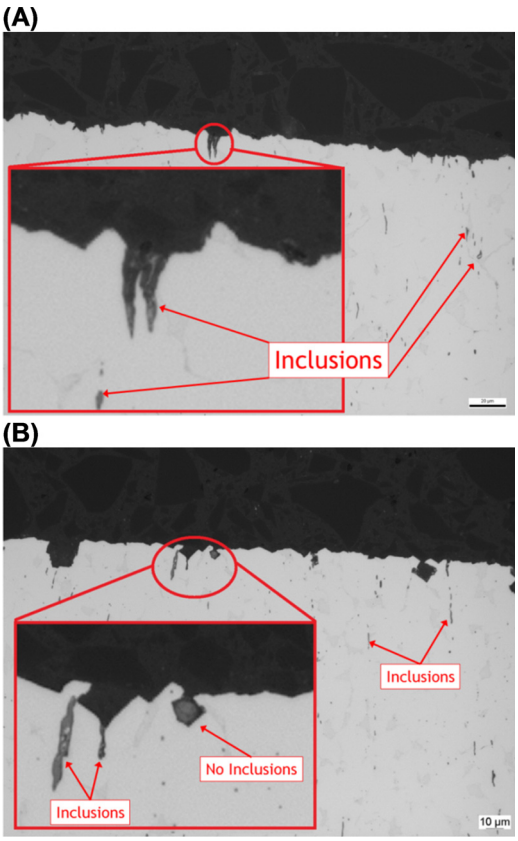

Fig. 22. Cross-sections micrographs of 12 o'clock positioned specimen exposed in cell D (inoculation with *Desulfovibrio desulfuricans*) for 2200 h after corrosion product removal: (A) Micrograph showing beginning of corrosion attack on location of MnS inclusion; (B) Micrograph showing beginning of corrosion attack in presence and absence of MnS inclusion.

S275JR. On the etched cross section of the two specimens, selective attack in the vicinity of inclusion lines can be identified (Fig. 21). However a correlation cannot be clearly shown between a corrosion pit and the presence of an inclusion. The corrosion pits in general show a dependency on the crystallographic orientation, which can be deduced from their square or rectangular appearance in the SEM images and from the rather straight boundaries of the pits in the cross section. This is not surprising knowing that bacterial initial attachment occurs on or in the proximity of the grain boundaries. This phenomenon has origin in differential energy distribution between the grain boundaries and matrix [2,51], resulting in higher energy allocated in grain boundaries that attract bacteria [51]. Therefore, it is expected that initial localized material deterioration will occur also on grain boundaries as shown in the presented micrograph.

Investigation centered on influence of MnS inclusion on corrosion attack provides inconclusive results. In Fig. 22A and B it is possible to observe beginning of corrosion attack at location of inclusion. In that case the inclusion shows the typical linear appearance of MnS. On the contrary, lack of this mechanism is recorded on Fig. 22B; the inclusion at the onset of corrosion is of circular shape (e.g. oxidic). The remaining corrosion pits are free of nonmetallic inclusions, which might be due to the advanced state of corrosive attack.

From material structure it is possible to see that corrosion initiation is attracted to grain boundaries and inclusions. Yet, to gain more information it is required to study these processes in a short period after environment inoculation. It may be the case that MnS inclusions play role in the localized corrosion initiation [20,21]. Nonetheless, their role in further development of corrosion attack with time is attenuate.

4. Conclusion

Herein presented results show that the presence of sulfidogenic species in the seawater environment may result in degradation of the surface of carbon steel, leading to a rougher surface topography as well as localized corrosion damage. However, a long-term exposure in systems where the high bacterial activity was recorded does not have to necessary result in elevated corrosion rates, as has been previously reported. The formation of the observed corrosion attack pattern was investigated for two influencing factors:

(a) Influence of the material surface microstructure on the degradation topography:

The influence of the steel surface microstructure in the observed deterioration process and impact on the damage layout is recognized. Grain boundaries and inclusions (e.g. MnS) are playing a significant role during the initial stage of corrosion attack (pit initiation), although this can diminish during latter stages of corrosion and material degradation as shown in the work presented herein.

(b) Impact of environment established on the material surface:

Microbial activity is affecting the mineralization process naturally occurring on the carbon steel surface leading to architectures composed of mixed iron(II) and (III) minerals such as iron sulfides, magnetite, iron oxyhydroxides, chukanovite and sulfated and carbonated green rust as well as calcareous deposits. Inner layers of these structures could possibly provide an anaerobic habitat

for SRBs, where they can flourish by utilization of sulfate form GR(SO_4^{2-}) as a terminate electron acceptor for their dissimilarity respiration which enables continuous degradation of steel.

Study about mitigation of the microbial hazard in these particular environmental conditions showed that the impact of antimicrobial treatment on a planktonic microbial population is positive even in lower concentrations than typically applied. Consequences of antimicrobial treatment in this case collide with its intended function; to stop biological reaction and the production of aggressive metabolic products (S^{2-}, $S_2O_3^{2-}$, etc...), and therefore decreases general material deterioration. However, the microbial population on the steel surface can be protected by corrosion products and cannot be always reached by antimicrobial product, which implies continuous material deterioration in some regions of material surface. Moreover, with a new available source of energy and electron acceptor, microorganisms, either sessile or planktonic, have the possibility to reinstall their activities which could lead to further material deterioration.

Acknowledgments

Funding was received from the European Community's Seventh Framework Programme (FP7/2007–2013). The authors wish to express their gratitude towards Øystein Birketveit from MISWACO, A Schlumberger Company, Anne Karin Nyhaug and Endy Spriet from Molecular Imaging Center in Bergen, Leonardo Dall'Agnol and Prof. Jose Moura from Faculdade de Ciências e Tecnologia Universidade Nova de Lisboa in Lisbon, and to Dr. Marie Libert and Marta Kerber Schutz from CEA in Cadarache for their support in the production of presented work.

References

[1] W. Lee, Z. Lewandowski, P.H. Nielsen, W.A. Hamilton, Role of sulfate-reducing bacteria in corrosion of mild steel: A Review, Biofouling 8 (1995) 165.
[2] R. Javaherdashti, Microbiologically Influenced Corrosion: An Engineering Insight, Springer-Verlag, London, 2008.
[3] H.A. Videla, Electrochemical interpretation of the role of microorganisms in corrosion, in: D.R. Houghton, R.N. Smith, H.O.W. Eggins (Eds.), Biodeterioration, 7, Elsevier Applied Science, London, 1988, p. 359.
[4] Z. Szklarska-Smialowska, Pitting Corrosion of Metals, NACE International, Houston, 1986.
[5] C.A.H. Von Wolzogen Kühr, L.S. Van der Vlugt, Graphication of cast iron as an electrochemical process in anaerobic soils, Water 18 (1934) 147.
[6] R.D. Bryant, E.J. Laishley, The role of hydrogenase in anaerobic biocorrosion, Canadian Journal of Microbiology 36 (1990) 259.
[7] I. Pankhania, Hydrogen metabolism in sulphate-reducing bacteria and its role in anaerobic corrosion, Biofouling 1 (1988) 27.
[8] R.D. Bryant, E.J. Laishley, The effect of inorganic phosphate and hydrogenase on the corrosion of mild steel, Microbiology and Biotechnology 38 (1993) 824.
[9] R.D. Bryant, W. Jansen, J. Boivin, E.J. Laishley, J.W. Costerton, Effect of Hydrogenase and Mixed Sulfate- Reducing Bacterial Populations on the Corrosion of Steel, Applied Environmental Microbiology 57 (1991) 2804.
[10] S. Da Silva, R. Basséguy, A. Bergel, Electrochemical deprotonation of phosphate on stainless steel, Electrochimica Acta 49 (2004) 4553.
[11] L. De Silva Munoz, A. Bergel, R. Basséguy, Role of the reversible electrochemical deprotonation of phosphate species in anaerobic biocorrosion of steels, Corrosion Science 49 (2007) 3988.
[12] R. Cord-Rustwich, Microbially influenced corrosion of steel, in: D.R. Lovely (Ed.), Environmental Microbe–Metal Interactions, ASM Press, Washington DC., 2000, p. 159, Ch. 7.
[13] R.A. King, J.D.A. Miller, Corrosion by the Sulphate-reducing Bacteria, Nature 233 (1971) 491.
[14] R.A. King, J.D.A. Miller, J.S. Smith, Corrosion of Mild Steel by Iron Sulphides, British Corrosion Journal 8 (1973) 137.
[15] B.S. Rajagopal, J. LeGall, Utilization of cathodic Hydrogen by Hydrogen-Oxidizing Bacteria, Applied Microbiology and Biotechnology 31 (1989) 406.
[16] W.A. Hamilton, W. Lee, Biocorrosion, in: L.L. Barton (Ed.), Sulfate Reducing Bacteria, Plenum Press, New York, 1995, p. 243.
[17] I.B. Beech, C.W.S. Cheung, Interactions of exopolymers produced by sulphate-reducing bacteria with metal ions, International Biodeterioration and Biodegradation 35 (1995) 59.
[18] T.E. Ford, J.S. Maki, R. Mitchell, Involvement of bacteria exopolymers in biodeterioration of metal, in: D.R. Houghton, R.N. Smith, H.O.W. Eggins (Eds.), Biodeterioration, 7, Elsevier Applied Science, London, 1988, p. 378.
[19] W.A. Hamilton, Microbially influenced corrosion as a model system for the study of metal microbe interactions: a unifying electron transfer hypothesis, Biofouling 19 (1) (2003) 65.
[20] H. Castaneda, X.D. Benetton, SRB-biofilm influence in active corrosion sites formed at the steel-electrolyte interface when exposed to artificial seawater conditions, Corrosion Science 50 (2008) 1169.
[21] H.A. Videla, L.K. Herrera, R.G. Edyvean, An updated overview of SRB influenced corrosion and protection of carbon steel, in: CORROSION 2005, NACE International, Houston, USA, 2005, Paper no. 05488.
[22] I.B. Beech, J. Sunner, Biocorrosion: towards understanding interactions between biofilms and metals, Current Opinion in Biotechnology 15 (2004) 181.
[23] K. Alain, P. Pignet, M. Zbinden, M. Quillevere, F. Duchiron, J.P. Donval, F. Lesongeur, G. Raguenes, P. Crassous, J. Querellou, M.A. Cambon-Bonavita, Caminicella sporogenes gen. nov., sp. nov., a novel thermophilic spore-forming bacterium isolated from an East-Pacific Rise hydrothermal vent, International Journal of Systematic and Evolutionary Microbiology 52 (2002) 1621.
[24] O.A. Ramos Monroy, M.J. Hernández Gayosso, N. Ruiz Ordaz, G. Zavala Olivares, C. Juárez Ramírez, Corrosion of API XL 52 steel in presence of *Clostridium celerecrescens*, Materials and Corrosion 62 (9) (2011) 878.
[25] C. Cote, Ph.D. Thesis: Biocorrosion of Carbon Steel in Water Injection Systems of the Oil and Gas Industry: New Experimental Models from the Field, Université de Toulouse—MEGEP, Toulouse, 2013.
[26] G. Wranglen, Active sulfides and the pitting corrosion of carbon steels, in: R.W. Staehle (Ed.), International Conference on Localized Corrosion proceedings, Williamsburg, U.S.A. 6–10 December, NACE International, 1971, p. 462.
[27] G. Wranglen, Pitting and sulphide inclusions in steel, Corrosion Science 4 (1974) 331–349.
[28] R. Avci, B.H. Davis, M.L. Wolfenden, I.B. Beech, K. Lucas, D. Paul, Mechanism of MnS-mediated pit initiation and propagation in carbon steel in an anaerobic sulfidogenic media, Corrosion Science 76 (2013) 267.
[29] B.J. Little, J.S. Lee, Microbiologically Influenced Corrosion, John Wiley and Sons Inc., New Jersey, 2007.
[30] F. Mansfeld, B.J. Little, A technical review of electrochemical techniques applied to microbiologically influenced corrosion, Corrosion Science 3 (2) (1991) 247.
[31] J.S. Lee, R.I. Ray, E.J. Lemieux, M.N. Tamburri, B.J. Little, An evaluation of carbon steel corrosion under stagnant seawater conditions, Biofouling 20 (4/5) (2004) 237.
[32] W.P. Iverson, Transient Voltage Changes Produced in Corroding Metals and Alloys, Journal Electrochemical Society 115 (1968) 617.
[33] W.P. Iverson, G.J. Olson, L.E. Heverly, The role of phosphorus and hydrogen sulfide in the anaerobic corrosion of the iron and the possible detection of this corrosion by an electrochemical noise technique, in: S.C. Dexter (Ed.), Biologically Induced Corrosion, NACE International, Huston, 1986, p. 154.
[34] F. Huet, N. Monfort Moros, R.P. Nogueir, B. Tribollet, Electrochemical noise analysis applied to SRB-induced corrosion of carbon steel, in: CORROSION 2002, NACE International, Denver, USA, 2002, paper. no. 02449.
[35] A. Padilla-Viveros, E. Garcia-Ochoa, D. Alazard, Comparative electrochemical noise study of the corrosion process of carbon steel by the sulfate-reducing bacterium Desulfovibrio alaskensis under nutritionally rich and oligotrophic culture conditions, Electrochimica Acta 51 (2006) 3841.
[36] V.V. Zinkevich, I.B. Beech, Screening of sulfate-reducing bacteria in colonoscopy samples from healthy and colitic human gut mucosa, FEMS Microbiology Ecology 34 (2000) 147.
[37] M. Stern, A.L. Geary, Electrochemical Polarization. I. A Theoretical Analysis of the Shape of the Polarization Curves, Journal of Electrochemical Society 104 (1957) 56.
[38] R.A. Cottis, S. Turgoose, Electrochemical impedance noise, in: B.C. Syrett (Ed.), Corrosion Testing Made Easy Series, NACE International, Houston, 1999.
[39] X. Jiang, S. Nešić, Electrochemical investigation of the role of Cl^- on localized CO_2 corrosion of mild steel, in: 17th International Corrosion Congress, Las Vegas, USA, NACE International, 2008, paper no. 2414.
[40] S. Pineau, R. Sabot, L. Quillet, M. Jeannin, C. Caplat, I. Dupont-Morral, P. Refait, Formation of the Fe(II–III) hydroxysulphate green rust during marine corrosion of steel associated to molecular detection of dissimilatory sulphite-reductase, Corrosion Science 50 (2008) 1099.
[41] P. Refait, D.D. Nguyen, M. Jeannin, S. Sablé, M. Langumier, R. Sabot, Electrochemical formation of green rusts in deaerated seawater-like solutions, Electrochimica Acta 56 (2011) 6481.
[42] P. Refait, M. Jeannin, R. Sabot, H. Antony, S. Pineau, Electrochemical formation and transformation of corrosion products on carbon steel under cathodic protection in seawater, Corrosion Science 71 (2013) 32.
[43] C.O. Obuekwe, D.W.S. Westlake, J.A. Plambeck, Bacterial corrosion of mild steel under the condition of simultaneous formation of ferrous and sulphide ions, Applied Microbiology and Biotechnology 26 (1987) 294.
[44] G.H. Booth, A.W. Cooper, P.M. Cooper, Rates of microbial corrosion in continuous culture, Chemistry and Industry 86 (1967) 2084.
[45] G.H. Booth, A.W. Cooper, P.M. Cooper, Criteria of soil aggressiveness towards buried metals. II. Assessment of various soils, British Corrosion Journal 2 (1967) 109.
[46] P. Refait, M. Abdelmoula, J.-M.R. Génin, R. Sabot, Green rusts in electrochemical and microbially influenced corrosion of steel, Comptes Rendus Geoscience 338 (2006) 476.
[47] R. Galvan-Martinez, G. Garcia-Caloca, R. Duran-Romero, R. Torres-Sanchez, J. Mendoza-Flores, J. Genesca, Comparison of electrochemical techniques during the corrosion of X52 pipeline steel in the presence of sulfate reducing bacteria (SRB), Materials and Corrosion 10 (2005) 56.

[48] T. Nishimura, J. Dong, Corrosion Behavior of Carbon Steel for Overpack in Groundwater containing Bicarbonate Ions, Journal of Power and Energy Systems 3 (2009) 23.
[49] P. Refait, J.A. Bourdoiseau, M. Jeannin, D.D. Nguyen, A. Romaine, R. Sabot, Electrochemical formation of carbonated corrosion products on carbon steel in deaerated solutions, Electrochimica Acta 79 (2012) 210.
[50] H. Möller, E.T. Boshoff, H. Froneman, The corrosion behaviour of a low carbon steel in natural and synthetic seawater, The Journal of The South African Institute of Mining and Metallurgy 106 (2006) 585.
[51] K.R. Sreekumari, K. Nandakumar, Y. Kikuchi, Bacterial attachment to stainless steel welds: Significance of substratum microstructure, Biofouling 17 (2001) 303.